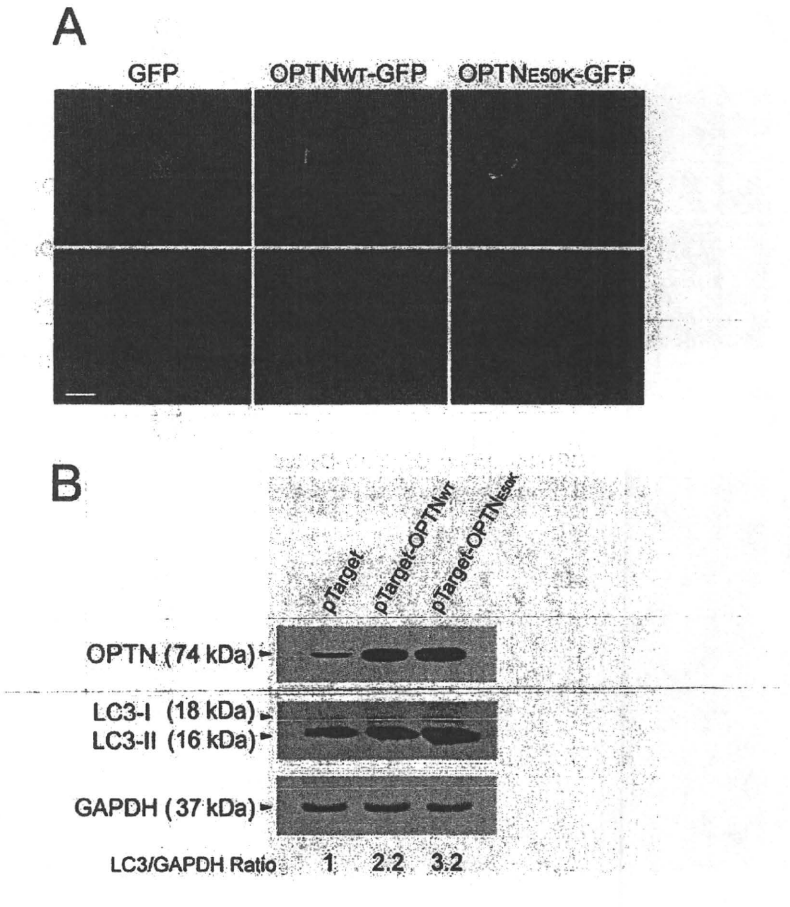

Figure 5

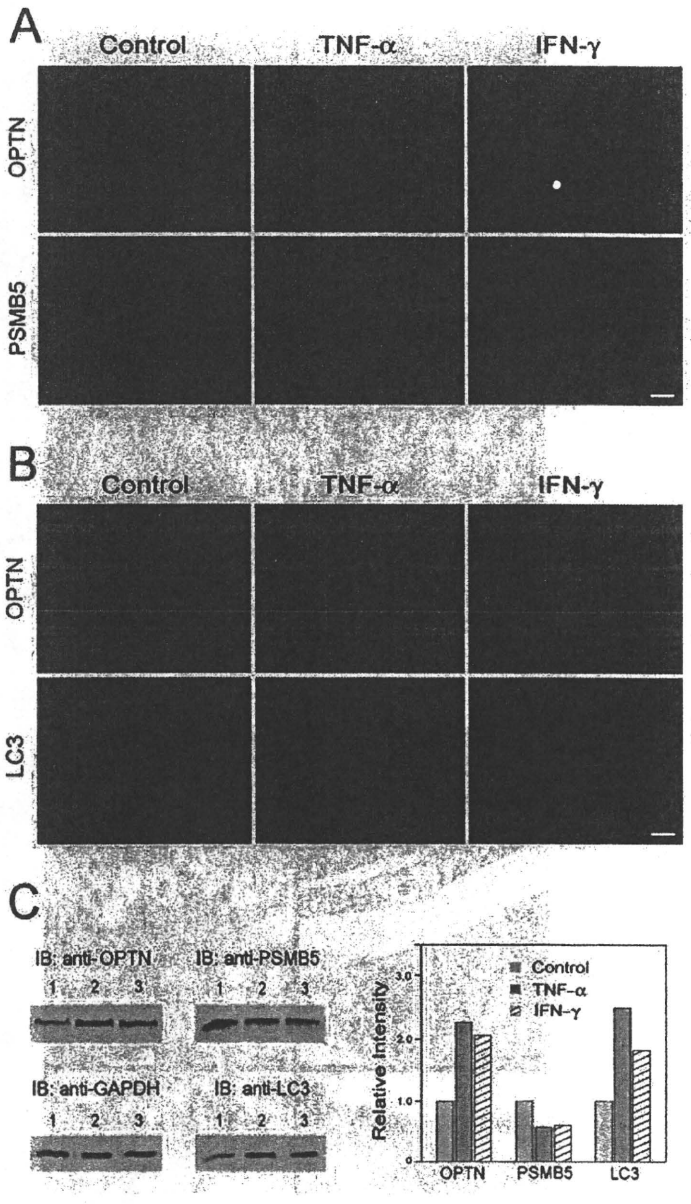

Figure 6

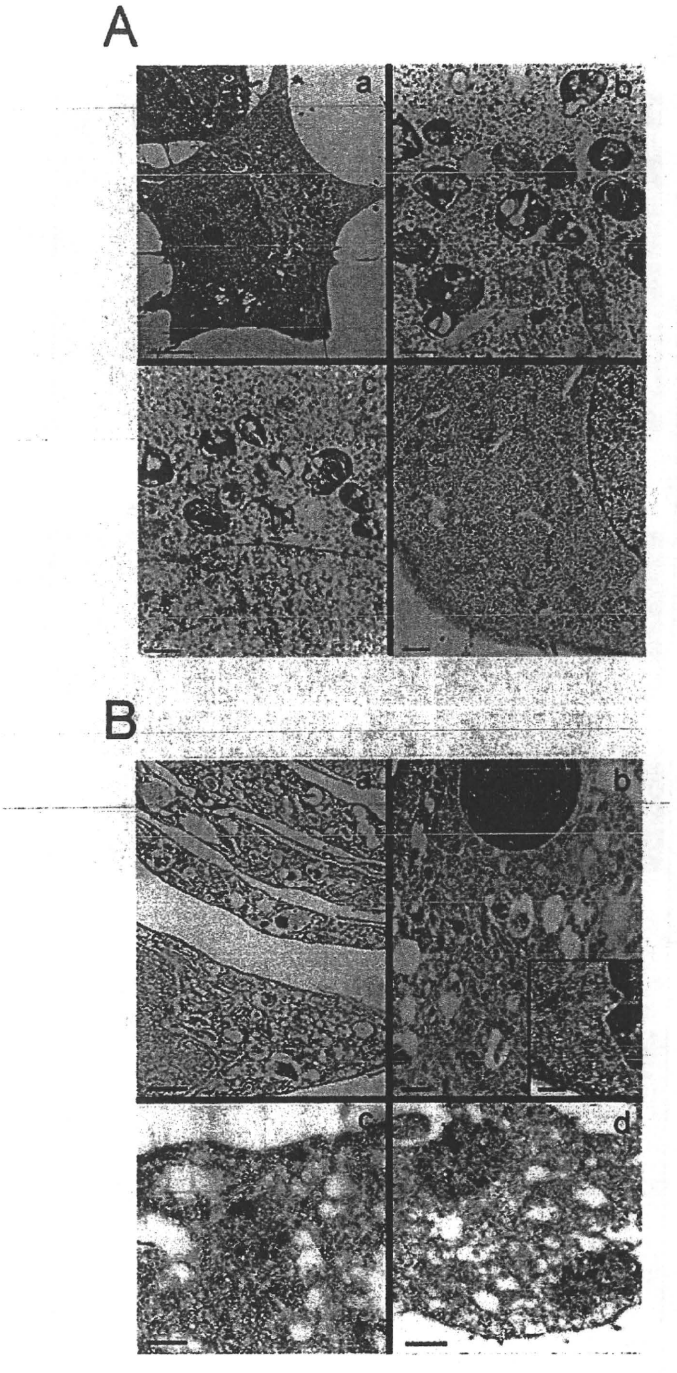

Figure 7

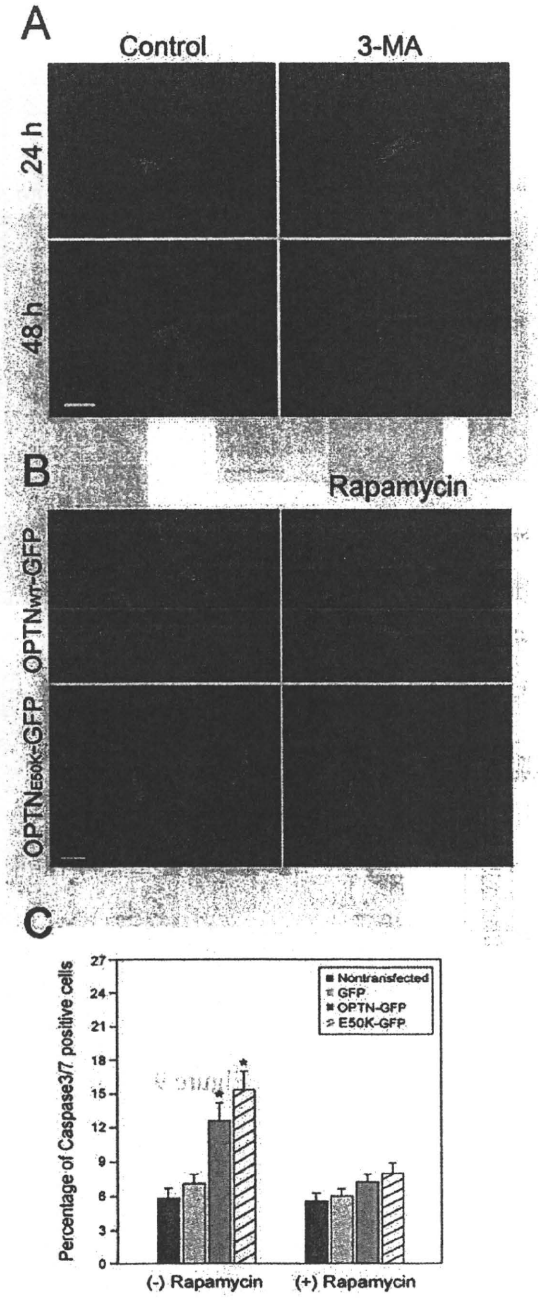

Figure 8

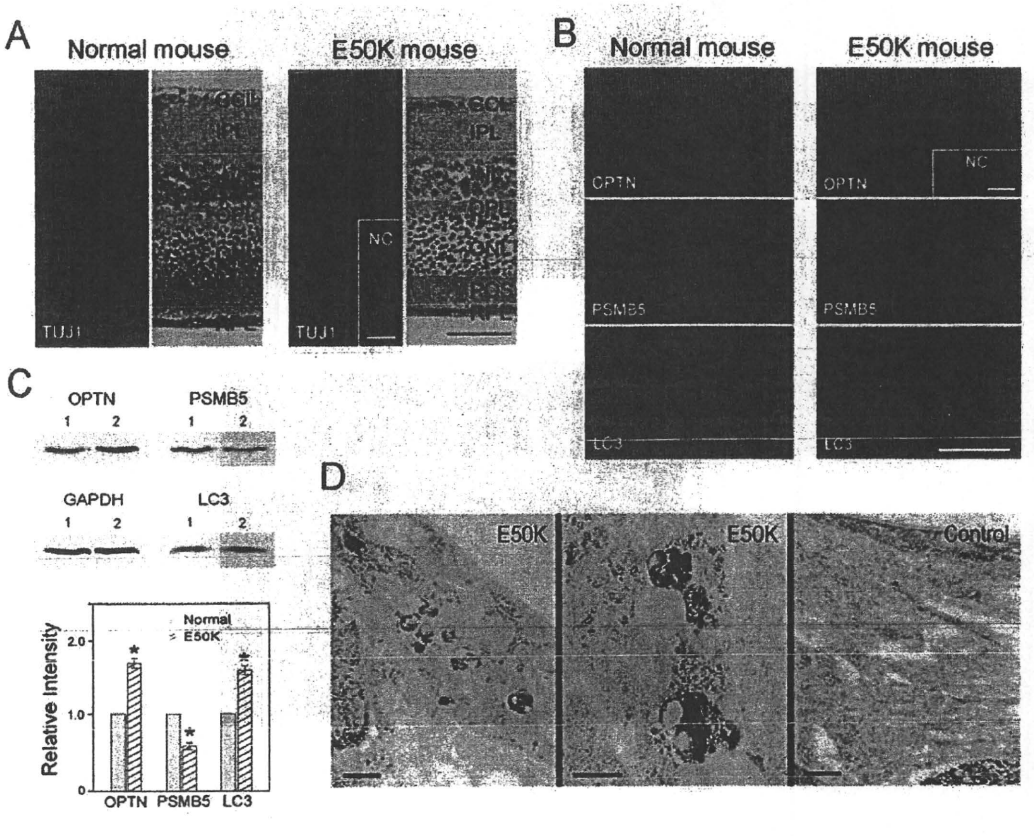
A
Normal mouse
E50K mouse
TUJ1
NC
B
Normal mouse
E50K mouse
OPTN
PSMB5
LC3
NC
C
OPTN
PSMB5
GAPDH
LC3
1 2
Normal
E50K
Relative Intensity
2.0
1.0
0
OPTN PSMB5 LC3
D
E50K
E50K
Control

Figure 9

OPEN ACCESS Freely available online

PLoS one

VAV2 and *VAV3* as Candidate Disease Genes for Spontaneous Glaucoma in Mice and Humans

Keiko Fujikawa[1,3,6]*, Takeshi Iwata[2], Kaoru Inoue[3], Masakazu Akahori[2], Hanako Kadotani[1], Masahiro Fukaya[4], Masahiko Watanabe[4], Qing Chang[5], Edward M. Barnett[5], Wojciech Swat[6]

1 Department of Pathology and Immunology, Hokkaido University Graduate School of Medicine, Sapporo, Japan, **2** National Institute of Sensory Organs, National Hospital Organization Tokyo Medical Center, Tokyo, Japan, **3** Faculty of Health Science, Hokkaido University, Sapporo, Japan, **4** Department of Anatomy, Hokkaido University Graduate School of Medicine, Sapporo, Japan, **5** Department of Ophthalmology and Visual Sciences, Washington University School of Medicine, St. Louis, Missouri, United States of America, **6** Department of Pathology and Immunology, Washington University School of Medicine, St. Louis, Missouri, United States of America

Abstract

Background: Glaucoma is a leading cause of blindness worldwide. Nonetheless, the mechanism of its pathogenesis has not been well-elucidated, particularly at the molecular level, because of insufficient availability of experimental genetic animal models.

Methodology/Principal Findings: Here we demonstrate that deficiency of Vav2 and Vav3, guanine nucleotides exchange factors for Rho guanosine triphosphatases, leads to an ocular phenotype similar to human glaucoma. Vav2/Vav3-deficient mice, and to a lesser degree Vav2-deficient mice, show early onset of iridocorneal angle changes and elevated intraocular pressure, with subsequent selective loss of retinal ganglion cells and optic nerve head cupping, which are the hallmarks of glaucoma. The expression of Vav2 and Vav3 tissues was demonstrated in the iridocorneal angle and retina in both mouse and human eyes. In addition, a genome-wide association study screening glaucoma susceptibility loci using single nucleotide polymorphisms analysis identified *VAV2* and *VAV3* as candidates for associated genes in Japanese open-angle glaucoma patients.

Conclusions/Significance: Vav2/Vav3-deficient mice should serve not only as a useful murine model of spontaneous glaucoma, but may also provide a valuable tool in understanding of the pathogenesis of glaucoma in humans, particularly the determinants of altered aqueous outflow and subsequent elevated intraocular pressure.

Citation: Fujikawa K, Iwata T, Inoue K, Akahori M, Kadotani H, et al. (2010) *VAV2* and *VAV3* as Candidate Disease Genes for Spontaneous Glaucoma in Mice and Humans. PLoS ONE 5(2): e9050. doi:10.1371/journal.pone.0009050

Editor: Patrick Callaerts, Katholieke Universiteit Leuven, Belgium

Received January 22, 2009; **Accepted** January 18, 2010; **Published** February 4, 2010

Funding: The work described in this report was funded in parts by a grant from the Ministry of Education, Culture, Sports, Science and Technology in Japan. The funders had no role in study design, data collection and analysis, decision to publish, or preparation of the manuscript.

Competing Interests: The authors have declared that no competing interests exist.

* E-mail: fujikawa@med.hokudai.ac.jp

Introduction

The critical importance of elevated intraocular pressure (IOP) in the pathogenesis of glaucomatous optic neuropathy is widely recognized [1,2]. While compromise of aqueous humor outflow is the key determinant of elevation in IOP [3,4], the molecular mechanisms underlying changes in the outflow pathway that lead to elevated IOP remain to be elucidated. For this reason, mouse genetic knockout models of spontaneous glaucoma are highly sought after.

The Vav proteins are the best-characterized family of guanine nucleotide exchange factors (GEFs) that activates Rho guanosine triphosphatases (GTPases) in a phosphorylation-dependent manner [5]. Rho GTPases control cell behavior via regulating the specific filamentous actin structures involved in migration, adhesion, and morphogenesis, by acting as binary switches cycling between an inactive (GDP-bound) and active (GTP-bound) state [6]. The three mammalian Vav proteins, Vav1, Vav2, and Vav3, share a Dbl homology domain for their enzymatic activity as GEFs and contain a common structural array characteristic of proteins involved in signal transduction. Regardless of the structural similarity, Vav proteins differ in their tissue distribution. Vav1 is expressed specifically in lymphoid lineage cells, whereas Vav2 and Vav3 are more widely expressed [5,7]. Genetic approaches using knockout mice have provided valuable information on the function of Vav proteins *in vivo*. Vav proteins are crucial for the development and function of hematopoietic lineage cells such as lymphocytes, neutrophils, natural killer cells, and osteoclasts [8–16]. Individual Vav proteins exhibit both redundant and specialized functions. Despite the wide distribution of Vav2 and Vav3 proteins in mouse tissues, little is known about their specific function in non-hematopoietic cells.

While trying to better elucidate the functions of Vav2 and Vav3 in non-hematopoietic cells, we discovered that Vav2/Vav3-deficient mice have a significant ocular phenotype. Specifically, we show that Vav2/Vav3-deficient mice have elevated IOP, which eventually manifests as buphthalmos. Loss of Vav2 and Vav3 expression is associated with changes in the iridocorneal angle, with eventual chronic angle closure. The elevation of IOP in Vav2/Vav3-deficient mice is accompanied by an optic

neuropathy characterized by selective loss of retinal ganglion cells (RGCs) and optic nerve head (ONH) excavation and is therefore consistent with glaucoma. In addition, both *VAV2* and *VAV3* are shown to be susceptibility loci by single nucleotide polymorphisms (SNPs) study of Japanese primary open-angle glaucoma patients.

Results

Vav2/Vav3-Deficient Mice Develop Buphthalmos

Eyes of Vav2/Vav3-deficient ($Vav2^{-/-}Vav3^{-/-}$) mice were noted to develop buphthalmos starting between 6 and 12 weeks of age (Figure 1). This enlargement was typically seen unilaterally at first, with frequent bilateral involvement over the next 1–2 months, and continued enlargement until the mice were 6-months old. Eventually, some of the eyes, became atrophic and phthisical in appearance (Figure 1A). In order to confirm our initial observations, we measured the corneal diameters and weights of $Vav2^{-/-}Vav3^{-/-}$ mice eyes and compared them with age-matched wild-type mice eyes (Figure 1B). The examination clearly showed our observations were relevant. We observed 200 $Vav2^{-/-}Vav3^{-/-}$ mice at 6 months of age and almost 75% of them showed the enlarged eyes (Figure 1C). In addition, histological study indicated that there were no abnormal findings in the tissues both around the enlarged eyes such as inflammation, tumor, or hyperplasia, and in the thyroid of the $Vav2^{-/-}Vav3^{-/-}$ mice (data not shown).

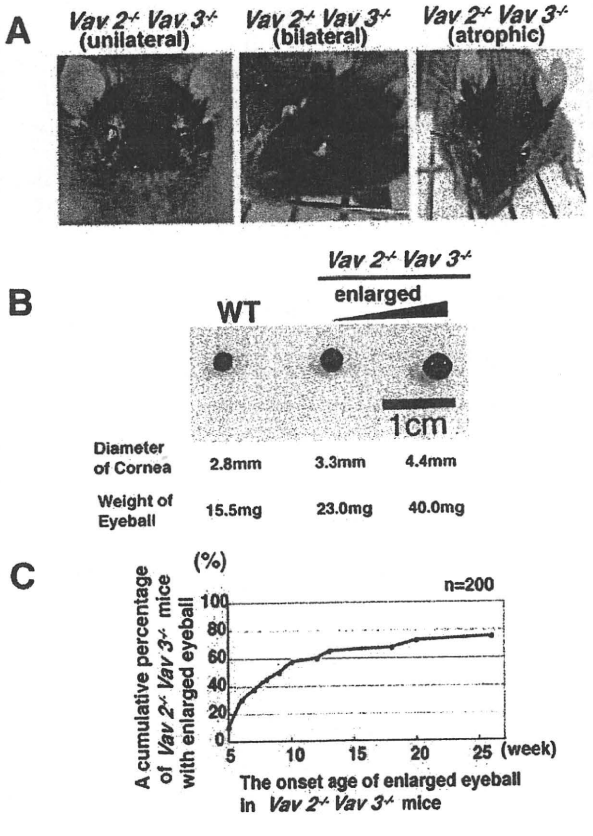

Figure 1. Vav2/Vav3-deficient mice develop buphthalmos. Eyes of Vav2/Vav3-deficient ($Vav2^{-/-}Vav3^{-/-}$) mice develop buphthalmos between 6 and 12 weeks of age. **A.** Left photo: Representative photo of unilateral enlarged eye in 10-week-old $Vav2^{-/-}Vav3^{-/-}$ mice. Centre photo: Representative photo of bilateral enlarged eyes in 16-week-old $Vav2^{-/-}Vav3^{-/-}$ mice. Right photo: Representative photo of enlarged eye becoming atrophic in 8-week-old $Vav2^{-/-}Vav3^{-/-}$ mice. **B.** Comparison of eye sizes. Left panel: Representative eye of 10-week-old wild-type (WT) mice as a control (n = 20). Cornea diameter is 2.9±0.1 mm. Weight is 15.8±1.1 mg. Centre panel: Representative first-recognized enlarged eye of $Vav2^{-/-}Vav3^{-/-}$ mice (9- to 10-week-old, n = 20). The cornea diameter is 3.3±0.1 mm. Weight is 23.7±4.4 mg. $P<0.001$. Right panel: Representative moderately enlarged eye of 12-week-old $Vav2^{-/-}Vav3^{-/-}$mice (n = 20). The cornea diameter is 4.2±0.4 mm. Weight is 38.0±4.0 mg. **C.** Age of onset of enlarged eyes up to 25 weeks of age in $Vav2^{-/-}Vav3^{-/-}$ mice (n = 200). The vertical axis is a cumulative percentage of $Vav2^{-/-}Vav3^{-/-}$ mice with enlargement of the eyes.
doi:10.1371/journal.pone.0009050.g001

Elevation of Intraocular Pressure of Vav-Deficient Mice

As we observed the development of buphthalmos, we assessed for elevated IOP in $Vav2^{-/-}Vav3^{-/-}$, Vav2-deficient ($Vav2^{-/-}$), and Vav3-deficient ($Vav3^{-/-}$) mice. IOP was measured using a rodent tonometer (Tonolab) starting at 4 weeks post-natal and were compared with age-matched wild-type C57BL/6 mice. Reliable measurement of IOP before 4 weeks of age was not possible. At 6 weeks of age, $Vav2^{-/-}Vav3^{-/-}$ mice first showed increased IOP (18.2±3.1 vs. 14.0±2.4 mmHg, $p<0.05$), with further increases out to 10 weeks of age (22.5±7.4 vs. 14.6±4.2 mmHg, $p<0.01$) (Figure 2A). IOP measurements in $Vav2^{-/-}Vav3^{-/-}$ mice ranged from 11–40 mmHg between 7 weeks and 16 weeks of age. There was a statistically significant difference in IOP between the $Vav2^{-/-}Vav3^{-/-}$ and wild-type mice at all time points demonstrated. The phenotype of littermate wild type mice was identical to that of the "inbred" C57BL/6 strain (Figure S1).

In $Vav2^{-/-}$ mice, elevated IOP was first detected at 7 weeks of age. The IOP for $Vav2^{-/-}$ mice was found to be increased at 8 weeks of age compared to wild-type mice (15.5±3.7 vs. 14.0±4.2 mmHg, $p<0.05$)(Figure 2B). The IOP of $Vav2^{-/-}$ mice showed further increases at 10 weeks of age (18.1±3.7 vs. 14.6±4.2 mmHg, $p<0.01$) and remained significantly higher at 12 weeks. In contrast, the IOP of $Vav3^{-/-}$ mice did not differ significantly from wild-type mice between 8 and 12 weeks (Figure 2C). The phenotype of littermate wild type mice was identical to that of inbred strain "C57BL/6". We also demonstrated that the phenotype of Vav2 and Vav3 heterozygous littermate mice ($Vav2^{+/-}$, and $Vav3^{+/-}$) were same as that of wild type (Figure S1).

Retinal Ganglion Cell Loss and Optic Nerve Head Changes in Vav2/Vav3-Deficient Mice

We next examined whether Vav2/Vav3-deficient ($Vav2^{-/-}Vav3^{-/-}$) mice showed changes in the retinal ganglion cell (RGC) layer and optic nerve head (ONH). At 3 weeks of age, $Vav2^{-/-}Vav3^{-/-}$ mice did not show any histological difference in the ONH or the number of RGCs compared to that of age-matched wild-type mice (Figure 3A). At 10 weeks of age, following several weeks of IOP elevation, early signs of ONH cupping and cell body loss in the RGC layer were apparent in $Vav2^{-/-}Vav3^{-/-}$ mice (Figure 3B). At 15 and 30 weeks of age, $Vav2^{-/-}Vav3^{-/-}$ mice showed further evidence of ONH cupping and RGC loss in the context of an otherwise normal retinal architecture. These findings are consistent with a selective loss of RGCs with corresponding changes in the ONH, which are the hallmarks of glaucoma.

Iridocorneal Angle Histopathology in Vav-Deficient Mice

As histopathological examination of globes from mice with buphthalmos frequently demonstrated angle closure, we compared

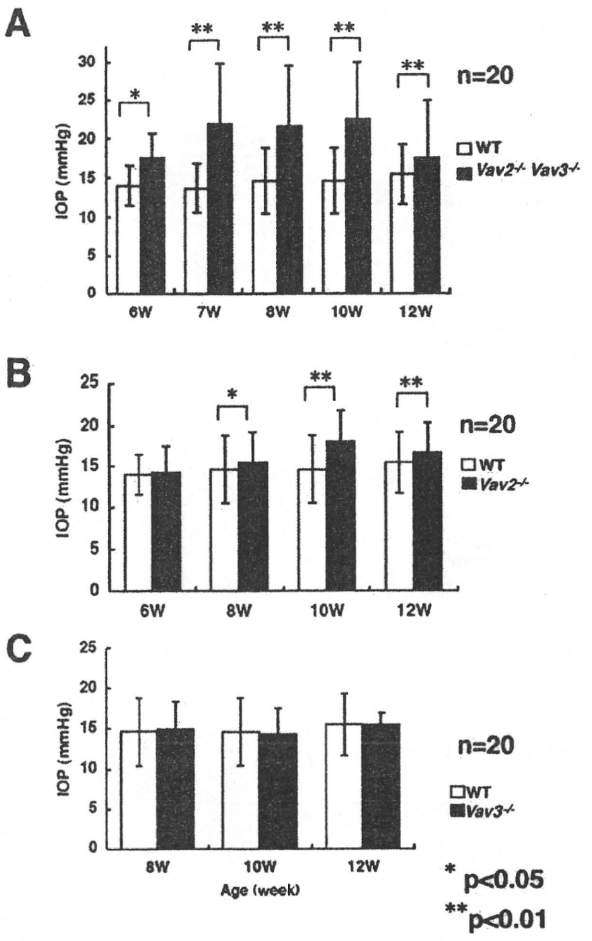

Figure 2. Elevated intraocular pressure of $Vav2^{-/-}Vav3^{-/-}$ and $Vav2^{-/-}$ mice. The intraocular pressure (IOP) of Vav2/Vav3-deficient ($Vav2^{-/-}Vav3^{-/-}$), Vav2-deficient ($Vav2^{-/-}$), and Vav3-deficient ($Vav3^{-/-}$) mice were measured between 10–12 AM. At the indicated ages, twenty mice were examined, respectively. For the IOP measurement of each Vav-deficient mouse, IOP of an age-matched wild-type (WT) mouse was also measured under the same conditions. We confirmed that these results were reproducible with four independent examinations. **A.** IOPs of $Vav2^{-/-}Vav3^{-/-}$ mice were dramatically elevated at 6 weeks of age. **B.** $Vav2^{-/-}$ mice also showed elevated IOP from around 8 weeks of age. **C.** $Vav3^{-/-}$ mice have normal range of IOP at any age. Error bars represent S.D. *P<0.05, **P<0.01 versus WT mice.
doi:10.1371/journal.pone.0009050.g002

the iridocorneal angle histology of 20 Vav2/Vav3-deficient ($Vav2^{-/-}Vav3^{-/-}$) mice with wild-type mice at both 7 and 12 weeks of age. Angles were classified as either being completely open, displaying evidence of partial occlusion of the trabecular meshwork (TM) as manifest by peripheral anterior synechiae (PAS), or being completely closed (total occlusion of the trabecular meshwork)(Figure 4A). Over half of the Vav2/Vav3-deficient mice already showed evidence of angle closure by 7 weeks of age, increasing to nearly 80% in 12-week-old mice (Figure 4B).

We also examined the correlation between elevated IOP and angle changes in 7-week-old $Vav2^{-/-}Vav3^{-/-}$ mice respectively (n = 20) (Figure S2). The mean and standard deviation of IOP in 7-week-old wild-type mice (n = 18) were 13.7±3.12 mmHg respectively. The 95th percentile of those IOPs using a normal curve was 18.8 mmHg. So that IOP over 18.8 mmHg was regarded as elevated IOP. $Vav2^{-/-}Vav3^{-/-}$ mice with elevated IOP showed evidence of angle closure by histological analysis, while $Vav2^{-/-}Vav3^{-/-}$ mice with non-elevated IOP displayed either open angles or evidence of early angle closure (PAS) and angle closure.

In addition, to characterize the progression of angle changes, two additional time points were added to this analysis of the iridocorneal angle −18 days and 4 weeks of age (n = 20 each). While at 18 days of age nearly half of the eyes demonstrated open angles, a large percentage already showed evidence of PAS (Figure 4B). By 4 weeks of age, $Vav2^{-/-}Vav3^{-/-}$ mice showed increasing frequencies of both PAS and angle closure. Taken as a whole, the data showed a gradual progression from open angles to PAS formation to closed angle from 18 days to 12 weeks.

The iridocorneal angles of Vav2-deficient ($Vav2^{-/-}$) and Vav3-deficient ($Vav3^{-/-}$) mice were examined histologically and graded in a similar manner. The iridocorneal angles of $Vav2^{-/-}$ mice also demonstrated evidence of progressive angle closure, but to a lesser extent as compared with $Vav2^{-/-}Vav3^{-/-}$ mice (Figure 4B). $Vav3^{-/-}$ mice had normal appearing open angles without evidence of PAS formation or angle closure (Figure 4B).

In order to better investigate the status of iridocorneal angles in $Vav2^{-/-}Vav3^{-/-}$ mice, we stained for myocilin as a marker for TM cells, as myocilin is strongly expressed in TM cells [17]. We examined 7-week-old $Vav2^{-/-}Vav3^{-/-}$ mice with non-elevated IOP who had either open angles or who displayed evidence of angle closure. As shown in Figure S3, myocilin was not detected in the iridocorneal angle of $Vav2^{-/-}Vav3^{-/-}$ mice with angle closure, but was seen in mice with open angles similar to those of wild-type mice.

Effects of Ocular Hypotensives in Vav2/Vav3 -Deficient Mice

We next tested the efficacy of ocular hypotensives used for human glaucoma in $Vav2^{-/-}Vav3^{-/-}$ mice with elevated IOP (Figure S4). The elevated IOP of 7-week-old $Vav2^{-/-}Vav3^{-/-}$ mice was dramatically reduced by ocular hypotensives used in humans, such as latanoprost, a prostaglandin analogue (Figure S4A). We also tested the IOP-lowering effect in $Vav2^{-/-}Vav3^{-/-}$ mice by two other ocular hypotensives, dorzolamide and timolol, whose mechanisms of action differ from that of latanoprost [18–20], being aqueous suppressants (Figure S4B). Furthermore, we tested Y-27632, a Rho-associated protein kinase inhibitor, that has been reported to cause a reduction in IOP presumably by altering cellular behavior of TM cells [21–23]. Y-27632 showed no effect of lowering IOPs against $Vav2^{-/-}Vav3^{-/-}$ mice, while it lowered the IOP significantly in age-matched wild-type mice (Figure S4C).

Expression of Vav2 and Vav3 in Mouse and Human Eyes

In order to understand the pathogenesis of the Vav2/Vav3-deficient eye phenotype, we examined the mRNA and protein expression patterns of Vav2 and Vav3 in the eye (Figure 5). Quantitative real-time PCR revealed that Vav2 and Vav3 mRNA are expressed in TM, cornea, retina, lens, iris, and ciliary body in the mouse eye (Figure 5A). Vav3 mRNA was more abundantly expressed than that of Vav2 in the TM and the retina. Gene expression levels of both Vav2 and Vav3 in the eye were comparable to levels found in immune cells where Vavs play a critical role [5,7–16]. Next, the Vav2 and Vav3 mRNA localization in mouse eye was examined by in situ hybridization (ISH) analysis (Figure 5B). Both Vav2 and Vav3 oligo probes (antisense), we used here, have been examined the specificities before and proved to have its specificity. As negative controls for

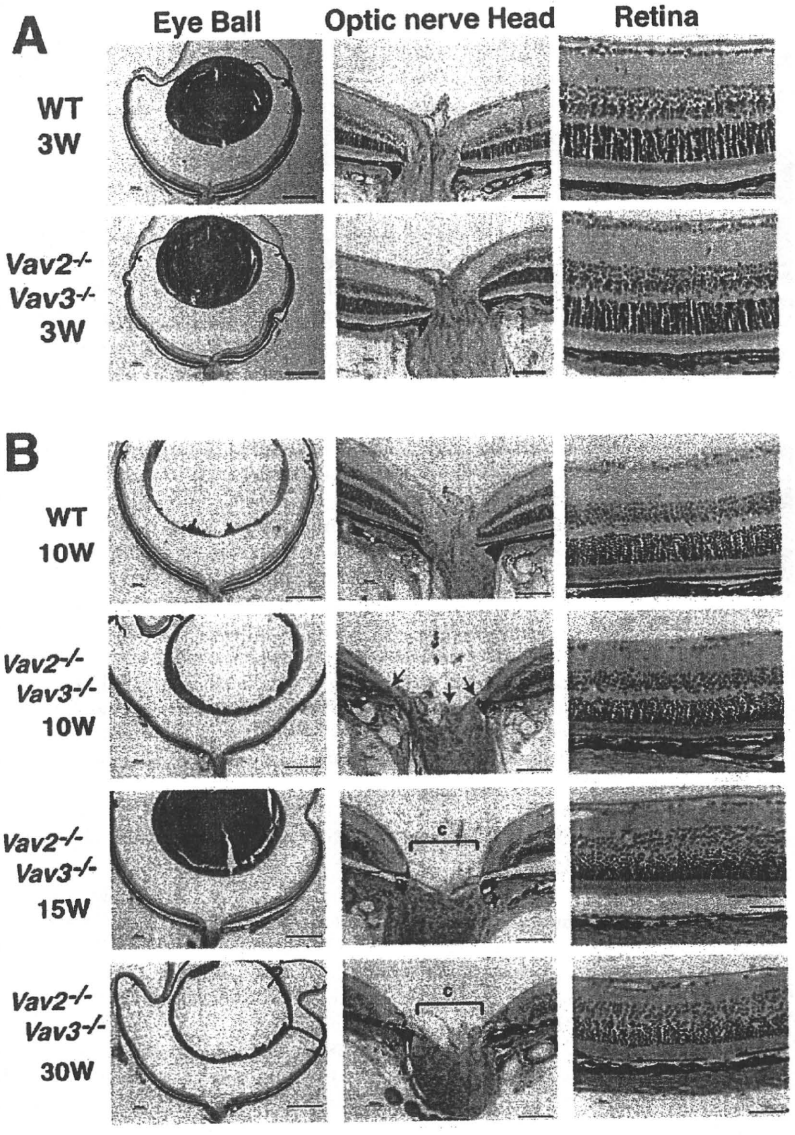

Figure 3. Optic nerve head degeneration and decrease in RGCs observed in $Vav2^{-/-}Vav3^{-/-}$ mice with elevated IOP. Light-microscopic histological examination is conducted to evaluate retinal neuropathy in Vav2/Vav3-deficient ($Vav2^{-/-}Vav3^{-/-}$) mice. **A.** At the age of 3 weeks, $Vav2^{-/-}Vav3^{-/-}$ mice exhibited impairment of angle status, but no abnormal findings of Optic nerve head degeneration (ONH) or retinal ganglion cells (RGCs) in the retinas. Scale bars, from left to right side: 500 μm, 100 μm, and 50 μm. **B.** After elevation of IOP, compared to control wild-type (WT) mice in the upper panel, ONH in 10-, 15-, and 30-week-old $Vav2^{-/-}Vav3^{-/-}$ mice present so-called capping (shown in c) and thin retinal neural layers (indicated by arrows in the photos). In those retinas, RGCs are decreased. Scale bars, from left to right side: 500 μm, 100 μm, and 50 μm. Sections are representative from 6–12 samples.
doi:10.1371/journal.pone.0009050.g003

these experiments, we used sense probes of Vav2 and Vav3, respectively, which showed no detectable signal (Figure S5). Both genes expression were widely distributed in the ocular tissues including the iridocorneal angle, retina, cornea, and sclera. The co- localization of Vav2 and Vav3 mRNA expression in iridocorneal angle, such as TM, was confirmed by ISH. Also, we assessed Vav2 and Vav3 protein expression by immunoblotting in both mouse and human eyes (Figure 5C). In mouse eyes, expression of both Vav2 and Vav3 was demonstrated in several ocular tissues including the iridocorneal angle, retina, cornea, and sclera. Both Vav2 and Vav3 proteins were also expressed in human retina and iridocorneal angle. The migrated bands were absent in the liver extracts of the $Vav2^{-/-}Vav3^{-/-}$ mice. Results of densitometric ratio (Vav3/Vav2) from normalized protein loading in each lane revealed that Vav3 was more abundantly expressed than Vav2 in the iridocorneal angle tissues of both mouse and human eyes and also in the retina.

Single Nucleotide Polymorphisms in Japanese Primary Open-Angle Glaucoma Patients

We observed Vav2 and Vav3 proteins expression in the tissues of human iridocorneal angle and retina. In order to investigate the

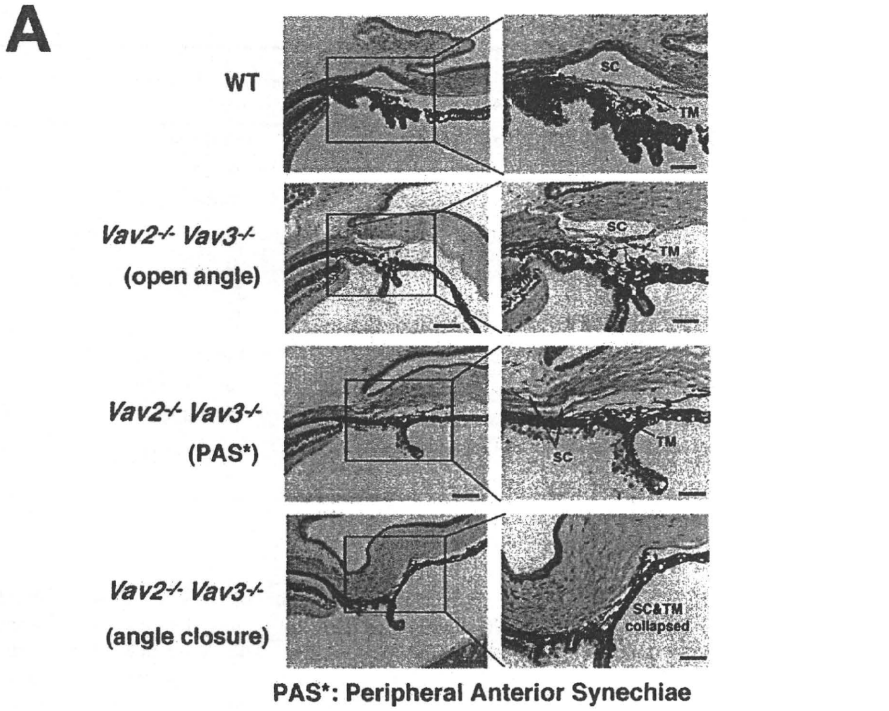

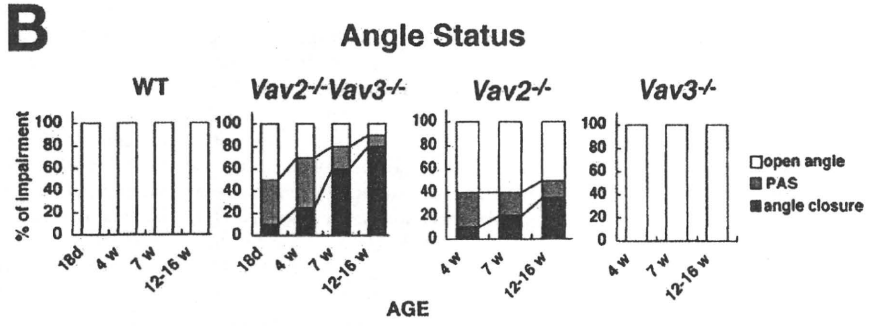

Figure 4. Characterization of progressive iridocorneal angle closures in $Vav2^{-/-}Vav3^{-/-}$ and $Vav2^{-/-}$ mice. The aqueous humor outflow facility, trabecular meshwork (TM) and Schlemm's canal (SC) (iridocornial angle) in Vav2/Vav3-deficient ($Vav2^{-/-}Vav3^{-/-}$) mice are evaluated in histological manner. Vav2-deficient ($Vav2^{-/-}$) mice also have the same changes, but of lower severity. **A.** Representative photos of normal TM and SC histology of 12-week-old wild-type (WT) mice as a control. Representative photos of normal open angle, peripheral anterior synechiae (PAS) in 12-week-old $Vav2^{-/-}Vav3^{-/-}$ mice, and angle closure status in 12-week-old $Vav2^{-/-}Vav3^{-/-}$ mice. Sections used here are all representative from 20 samples. Scale bars: left photos, 200 μm; right photos, 100 μm. **B.** Changes of angle status appear at the early ages. We classify angle status of $Vav2^{-/-}Vav3^{-/-}$, $Vav2^{-/-}$, and $Vav3^{-/-}$ mice into open angle, PAS, and angle closure by histological evaluation. We find the changes of angle status at the early ages, such as in 18-day-old $Vav2^{-/-}Vav3^{-/-}$ *mice* (n = 20) and in 4-week-old of $Vav2^{-/-}Vav3^{-/-}$ *mice* (n = 20). We took four ($Vav2^{-/-}Vav3^{-/-}$) and three ($Vav2^{-/-}$, $Vav3^{-/-}$) different age groups, with 20 mice examined, respectively.
doi:10.1371/journal.pone.0009050.g004

relevant association of *VAV2* and *VAV3* in human glaucoma patients, we carried out a genome-wide association study using the Affymetrix GeneChip Human Mapping 500 K Array Set. We examined Japanese primary open–angle glaucoma (POAG) cases and age-matched non-glaucoma controls. Both *VAV2* and *VAV3* loci in Japanese POAG patients showed SNPs against the non-glaucoma controls for dbSNPs rs2156323 and rs2801219, respectively. We reported the most extreme (Table 1). Both were intronic SNPs, SNP rs2156323 lying in intron3 of *VAV2* and SNP rs2801219 lying in intron1 of *VAV3*. *VAV2* SNP rs2156323 in particular indicated significant association with Japanese POAG, including a 5.65 heterozygote odds ratio (95% confidence interval (CI): 1.99–16.0), 4.34 heterozygote relative risk (95% CI: 1.72–10.44) and 4.38×10^{-4} genotypic *P* value with respect to risk allele A.

Judging from alleric *P*-values distribution for detecting *VAV2* ranking and genotypic *P*- values distribution for *VAV3* ranking, we observed that *VAV2* and *VAV3* showed high scores ($-\log_{10}(P)$) among approximately 380,000 SNPs analyzed in this study (Figure 6). On the contrary, *VAV1* showed no association with the POAG. These data strongly suggest that *VAV2* and *VAV3* genes are susceptibility loci in Japanese POAG.

Table 1. Vav2, Vav3, Vav1 association study for POAG using the Affymetrix GeneChip.

Gene	*VAV2*	*VAV3*	*VAV1*
SNP ID	rs2156323	rs2801219	rs2617815
Chromosome Location	9q34.1	1p13.3	19p13.2
Position	133750375	108214454	6746147
Genotypic *P* value	4.38×10^{-4}	5.42×10^{-4}	4.41×10^{-2}
Allele	AG	AC	AG
Risk allele	A	C	G
Minor allele	A	C	G
Heterozygote odds ratio (95%CI)	5.65 (1.99–16.0)	2.03 (1.01–4.09)	1.04 (0.52–2.08)
Heterozygote relative risk (95%CI)	4.34 (1.72–10.44)	1.31 (1.00–1.75)	1.01 (0.82–1.23)
Homozygote odds ratio	Not Available	Not Available	Not Available
Exon Intron	*VAV2* Intron3	*VAV3* Intron1	*VAV1* Intron1
SNP type	iSNP*1	iSNP	iSNP

*1: intronic S.

doi:10.1371/journal.pone.0009050.t001

Discussion

To our knowledge, this is the first report of a spontaneous glaucoma phenotype in Vav2 ($Vav2^{-/-}$) or Vav2/Vav3-deficient ($Vav2^{-/-}Vav3^{-/-}$) mice. Vav2/Vav3-deficiency is associated with progressive iridocorneal angle changes and elevation of IOP in mice. Subsequent selective loss of RGCs and progressive ONH cupping are associated with this elevated IOP, as has previously been demonstrated in other rodent models of glaucoma [24]. The finding that Vav2-deficiency alone results in a glaucoma phenotype suggests that the absence of Vav2 plays a critical role in the development of this phenotype. Despite our finding that Vav3-deficiency did not result in either iridocorneal angle changes or elevated IOP, the more severe glaucomatous phenotype demonstrated in $Vav2^{-/-}Vav3^{-/-}$ mice as compared with $Vav2^{-/-}$ mice is consistent with an additive effect.

A number of induced glaucoma models have been established in rats and mice [24]. Each model has advantages and disadvantages, related to factors such as the ease of inducing elevated IOP, the magnitude, duration and variability of elevated IOP, and secondary effects on the eye. Due to the ease of genetic manipulation, mouse models are becoming increasingly popular over those in rats. Despite the lack of a lamina cribosa as found in human eyes, the mouse is a good genetic model to study the pathogenesis of human glaucoma as aqueous physiology and anterior segment anatomy are similar to that found in humans [25].

Other spontaneous models of glaucoma have been described in mice, most notably in DBA/2J mice. The pigmentary glaucoma phenotype demonstrated in the DBA/2J mice has been extensively studied at genetic, clinical, morphological and pathological levels [26–29]. A limitation of this model is that the elevated IOP phenotype is not primary but secondary due to the systemic pigment dispersion syndrome with the associated mutations in the *Gpnmb* and *Tyrp1* loci [26–30]. In these mice, recessive mutations in these 2 genes are associated with iris degeneration characterized by iris stromal atrophy and pigment dispersion with subsequent reduced outflow facility secondary to pigment and cell debris. Therefore, it is difficult to tie-in the identified mutations to the pathogenesis of any primary form of human glaucoma.

The Vav2/Vav3-deficient mouse has several characteristics which make it particularly useful as an animal glaucoma model. The elevated IOP occurs spontaneously in these genetically manipulated mice and does not require the ocular manipulation necessary in induced models. The frequency of the ocular phenotype is high and onset occurs at a relatively young age. In addition, ocular hypotensives commonly used to treat human glaucoma show efficacy in lowering IOP in this model. The most significant advantage of this mouse glaucoma model is that the deleted genes, Vav2 and Vav3, are well-focused targets that have been studied over 20 years providing a useful starting point for further investigation of the potential molecular mechanisms underlying this phenotype.

Several aspects of this model of spontaneous glaucoma will require further study and clarification, although we speculated from our histological results and the correlation between elevated IOP and angle status changes that anatomic angle closure is the possible mechanism for elevated IOP in this model. While progressive angle closure may be the etiology prior to elevated IOP in mice lacking Vav2 and Vav3 function, it may alternatively be a subsequent change related to other alterations in angle structures which might also affect aqueous humor outflow. In addition, since the expression of Vav2 and Vav3 was detected in ocular tissues other than those comprising the iridocorneal angle, it will be necessary in future studies to consider how their deficiency in these tissues might have potentially contributed to the spontaneous glaucoma phenotype in any way.

While so far there are several reports of glaucoma associated candidate genes based on the single nucleotide polymorphisms (SNPs) study in the Japanese population [31–36], our data first suggest that *VAV2* and *VAV3* are susceptibility loci in Japanese primary open–angle glaucoma (POAG) cases. In addition, so far we could not find the report of non-Japanese glaucoma association case study that demonstrated *VAV2* and/or *VAV3* as candidate gene loci for glaucoma [37–43]. They demonstrated glaucoma associated candidate genes study with SNPs analysis focusing on the other specific target genes, although we are interested in the *VAV2* and/or *VAV3* glaucoma association study using the different populations. This work would be important investigation to be done.

Although our current findings do not address the molecular mechanisms underlying glaucoma phenotypes, it is interesting to consider possible mechanisms based on what is currently known about Vav protein function. The TM has been regarded as a key determinant of IOP and has been implicated as the major site of

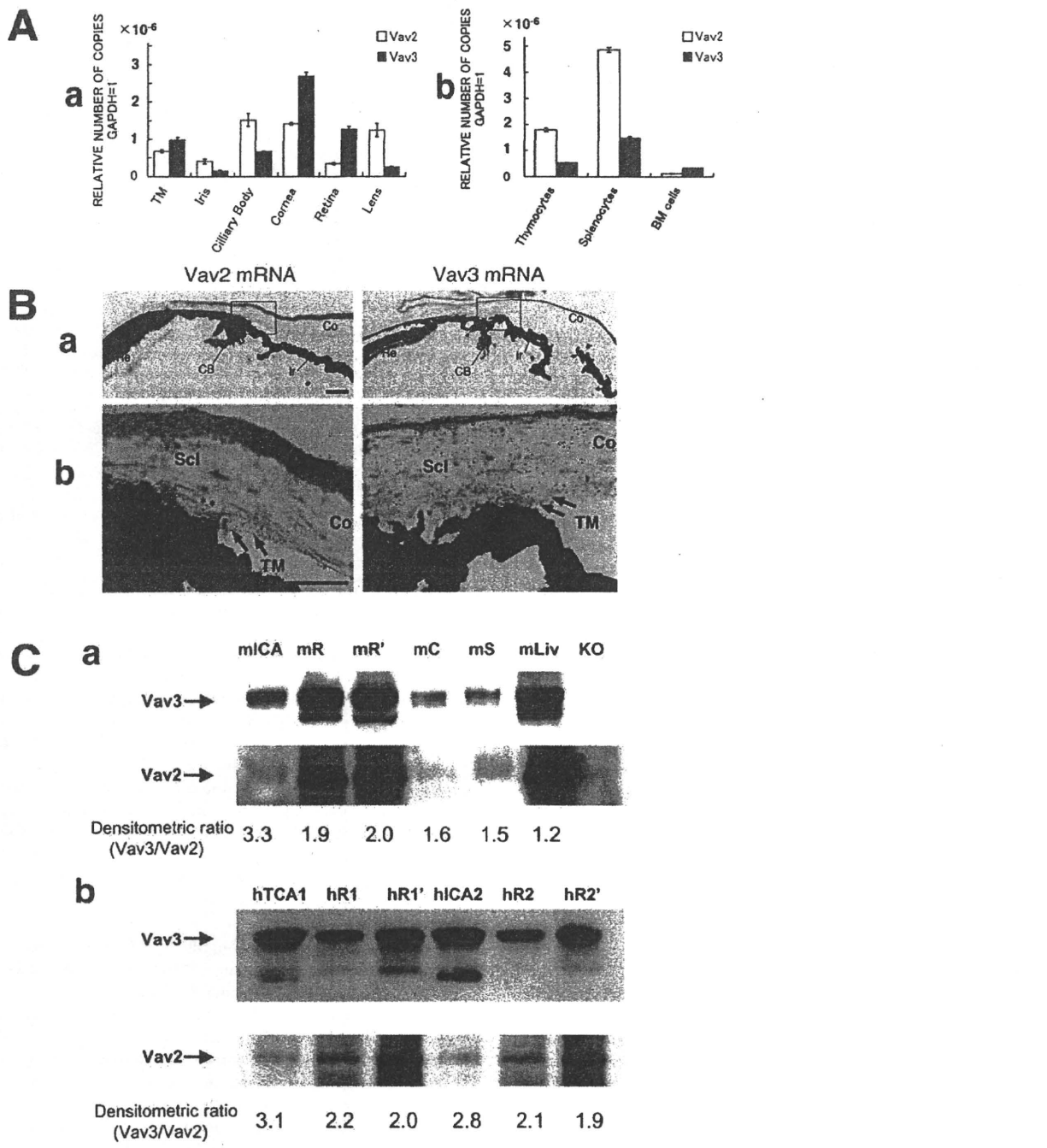

Figure 5. Vav2 and Vav3 expression in mouse and human eyes. A. Quantitative real time PCR analysis is performed for Vav2 and Vav3 mRNA expression study. The vertical axis is the copy number of Vav2 or Vav3 mRNA when that of mGAPDH is taken as 1. The assay method is absolute quantification (standard curve). **a.** Both Vav2 and Vav3 mRNA are expressed in all tissues of the murine eyes including the trabecular meshwork (TM), cornea, sclera, and retina. **b.** Vav2 and Vav3 mRNA expression level of murine immune cells. The levels of Vav2 and Vav3 expression in eye tissues are the same as those of the immune cells where Vav2 and Vav3 play the critical role. **B. a.** In situ hybridization analysis of emulsion-dipped sections display the distribution of Vav2 and Vav3 mRNA in the anterior chamber. The localization of Vav2 and Vav3 mRNA in trabecular meshwork(TM), ciliary body (CB), cornia(CO), iris(Ir), sclera (Scl) and retina(Re) by in situ hybridization. **b.** Vav2 and Vav3 mRNA expression are both detected in iridocorneal angle, such as TM (indicated by arrows in the photos). Scale bars, 50 μm. **C.** Expression of Vav2 and Vav3 proteins in mouse (**a**) and human (**b**) eyes. Vav2 and Vav3 proteins were detected in mouse or human ocular extracts (from two independent postmortem eye globe samples; at death age of 58 (1) and 87 (2)) by western blotting. Densitometric ratios (Vav3/Vav2) were shown under the blotting panels. mICA: mouse iridocorneal angle tissues, mR: mouse retina, mR': 3-fold increased loading mouse retina, mC: mouse cornea, mS: mouse sclera, mLiv: normal mouse liver(positive control), KO: Vav2/Vav3-deficient mouse as a negative control, hICA: human iridocorneal angle tissue,hR1: human retina 1, hR1': human retina1' (3-fold loading).
doi:10.1371/journal.pone.0009050.g005

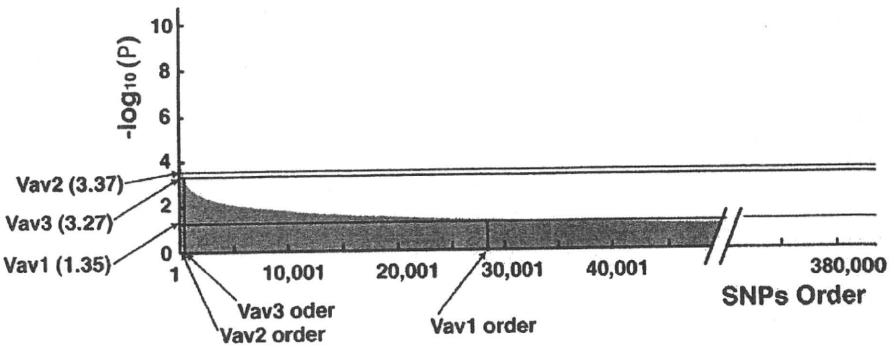

Figure 6. *VAV2* and *VAV3* genome-wide SNPs high ranking of *P*-value scores. Genome-wide ranking orders of *P*-value indicate that *VAV2* and *VAV3* are strongly susceptible genes with Japanese POAG cases. Clinically diagnosed Japanese POAG 100 cases and non-glaucoma age-matched 100 controls are examined for this study. The analysed SNPs number is about 380,000 by the Affymetrix GeneChip 500 K Mapping Array Set. The SNPs data under the 85% call rate, under 0.001 Hardy-Weinberg equilibrium (HWE), and under 5% minor allele frequencies are excluded. Allelic frequency $\chi 2$ test and genotypic frequency $\chi 2$ test are calculated respectively. The vertical axis is $-\log 10$ (*P*) and the horizontal axis is SNPs order which showed high scores from left to right. The Upper graph is alleric *P*-values distribution of *VAV2* analysis and the lower graph is genotypic *P*-values for *VAV3* and *VAV1* study. *VAV2* is located at high position in rank and *VAV3* also located at high position in rank. *VAV1* shows no association for POAG cases here.
doi:10.1371/journal.pone.0009050.g006

increased resistance to aqueous outflow which occurs in human glaucoma [44,45]. Recent findings indicate that signals emanating from integrins, key regulators of the actin cytoskeleton in trabecular meshwork cells, may be involved in control of outflow facility and Rho GTPases would be important downstream effectors of integrin-mediated actin cytoskeletal dynamics [4,46–48]. Considering the Vavs function as GEF, dysregulation of Rho is one possible mechanism by which pathology in the iridocorneal angle might result and is one that deserves further study.

In summary, we had demonstrated that Vav2/Vav3-deicient mice develop a spontaneous glaucoma phenotype. In addition, our data first suggest that *VAV2* and *VAV3* are susceptibility loci in Japanese primary open-angle glaucoma (POAG) cases. We believe that Vav2/Vav3-deficient mice will serve not only as a useful murine model of spontaneous glaucoma, but may also provide a valuable tool in understanding of the pathogenesis of glaucoma in humans, particularly the determinants of altered aqueous outflow and elevated IOP.

Materials and Methods

Mice

Vav3$^{-/-}$, *Vav2*$^{-/-}$ and *Vav2*$^{-/-}$*Vav3*$^{-/-}$ mice were described previously [15]. Mice were backcrossed at least 9 times with C57BL/6 mice (Clea Japan, Tokyo, Japan) to have the C57BL/6 background. All mice used in these experiments were bred and maintained in the SPF Facility of Hokkaido University Graduate School of Medicine in a 12-hour light-dark cycle. All mice experiments were approved by the Animal Ethics Committee of Hokkaido University Graduate School of Medicine and were conducted in accordance with the ARVO Statement for the Use of Animals in Ophthalmic and Vision Research.

Tissue Preparation and Histology

Eyes were quickly enucleated from each age group of knock-out mice and C57BL/6 wild-type control mice after deep anesthesia with pentobarbital sodium solution, then immediately fixed with solution of 2.5% glutaraldehyde (TAAB, EM Grade) in 10% formalin neutral buffer-methanol solution deodorized for anterior chamber study, or fixed with Davidson' solution for retinal analysis for 12 hours. Following this, the eyes were embedded in paraffin and dissected sagittally using a microtome into 5 μm sections. After deparaffinization and rehydration, the sections were stained with hematoxylin and eosin (Sigma).

Immunohistochemistry

The eyes were sectioned at 5 μm thickness along the vertical meridian through the optic nerve head. After deparaffinization and rehydration, the tissue sections were incubated with blocking solution containing 1% BSA in PBS for 1 hour. This was followed by 1 hour incubation with rabbit polyclonal antibody to myocilin at 1:200 in blocking solution as first antibody for 1 hour at room temperature. Anti-rabbit IgG conjugated with Alexa 488 (Molecular Probes, Eugene, OR) at 1:400 in PBS containing 0.1% Tween 20 was used as secondary antibody for 1 hour at room temperature. The stained tissues were examined using confocal fluorescence laser microscope (Radius 2000, Bio-Rad, Hercules, CA). For negative control of the immunohistochemical staining, the sections were incubated with blocking solution without primary antibody (data not shown).

Real Time PCR

Each tissue was freshly taken from SPF level C57BL/6 mice and immediately used for generating RNA by TRIzol reagent (Invitrogen). Templates for real time PCR were made by Cloned AMV Reverse Transcriptase (Invitrogen). Probes of mVav2 and mVav3 were TaqMan probes (Vav2: Mm00437287_m1, Vav3: Mm00445082_m1) purchased from Applied Biosystems (Foster city, CA). The standard curves were constructed by mVav2, mVav3 inserted plasmids, normalized by mGAPDH (Product Code: 4352339E, Applied Biosystems). All the PCR studies were performed by Applied Biosystems 7500 Real Time PCR System following the manufacturer's recommended procedures. The assay method was absolute quantification (standard curve).

In Situ Hybridization

The detailed procedure was described as previously [49]. Briefly, to detect mRNAs for Vav2 and Vav3, specific antisense oligonucleotide probes were synthesizedas follows:(2275–2319;45mers)5′-AGCTG-GAGACCGGCTTGAGGCC CTGCTGGTGGTTCGCTCCCG-AGA-3′ for Vav2 mRNA (GenBank accession No. NM_009500) and (2346–2302;45mers)5′–GTTGCCTGTTCTATTACCCCTCTG T CCAGCTGGCTGTTCTGGCTC-3′ for Vav3 mRNA (accession No. NM_020505). Oligonucleotide probes were labeled with [33P]

dATP using terminal deoxyribonucleotidyl transferase (Invitrogen, Carlsbad, CA). Under deep pentobarbital anesthesia, the eyeballs were freshly obtained from Adult C57BL/6J mice. Fresh frozen sections (20 μm thickness) were cut with a cryostat (CM1900, Leica, Nussloch,Germany) and mounted on glass slides precoated with 3-aminopropyltriethoxysilane. Sections were exposed to Nuclear Track emulsion (NTB-2, Kodak) for 5 weeks. Emulsion-dipped sections were stained with methyl green pyronine solution. The specificity of the hybridizing signals was verified by the disappearance of signals when hybridization was carried out with sense probes.

Western Blotting

Mouse Ocular Tissue Dissection: 8-week male C57BL/6J mice (Jackson Laboratory, ME) were used for ocular tissue samples. The animals were euthanized by carbon dioxide inhalation in an induction chamber. The globes were promptly enucleated after euthanization and washed in ice-cold PBS. Ocular tissues were microscopically dissected. Dissection of Postmortem Human Eye Globes: Human eyes without previous eye diseases including glaucoma were acquired from a local eye bank (Heartland Lions Eye Banks; Columbia, MO) within 6 hours post-mortem. Dissected mouse and postmortem human ocular tissues were lysed in a tissue extraction buffer (BioChain, CA). The concentration of protein supernatants was determined by a protein assay kit (Bio-Rad, CA). Rabbit polyclonal anti-mouse Vav2 (1:1000) (Santa Cruz Biotechnology, CA), monoclonal anti-human Vav2 (1:2000) (Cell Signaling Technology, MA), polyclonal anti-mouse and anti-human Vav3 (1:3000 for each) (Millipore, CA) antibodies were used for detection.

Intraocular Pressure (IOP) Measurement

IOP was measured using the TonoLab rebound tonometer for rodents (Tiolat i-care, Finland) according to the manufacturer's recommended procedures. All IOP measurements were performed between 10 AM and noon in conscious condition. Mice were gently restrained first by hand and placed on a soft towel bed on the desk and usually appeared calm and comfortable. These data were confirmed to be reproducible by three additional different independent studies (n = 20).

Evaluation of Eye Drop Medications for High Intra-Ocular Pressure of Vav2Vav3-Deficient Mice

Vav2$^{-/-}$*Vav3*$^{-/-}$ mice were housed in SPF barrier facility in standard lighting conditions (12-hour light-dark cycle). The 7–9 week after birth mice were used for the experiment. Four independent experiments were carried out to confirm the results reproducible.

Preparation and Application of Ophthalmic Solution

Latanoprost was purchased from Cayman Chemical Co. (Ann Arbor, MI) and dissolved in its vehicle solution (0.02% benzalkonium chloride, 0.5% monosodium phosphate monohydrate, 0.6% disodium hydrogen phosphate dihydrate and 0.4% sodium chloride). With a micropipette, 3 μl of PG analogue (latanoprost; prostaglandin F2α) solution or vehicle was randomly applied to the eyes of *Vav2*$^{-/-}$*Vav3*$^{-/-}$ mice. Before administration, IOP was measured with the tonometer from 10–12 AM and then the PG analogue 0.005% 3 μl or vehicle solution was applied in a masked manner. Evaluation of IOP-lowering effect was performed by measuring the IOP with the tonometer at 3 hours after drug instillation also in a masked manner. Furthermore, two different mechanistic medications, 3 μl of timolol maleate (0.5%, Merck, Whitehouse Station, NJ) or 3 μl of dorzolamide hydrochloride (1%, Trusopt; Merck), was also tested, respectively, after measuring the IOP under the same conditions as those of the Latanoprost application. Evaluation of IOP-lowering effects was performed by measuring the IOP with tonometer at 2 hours after drug instillation under blinded test protocols. Y-27632 was purchased from Carbiochem (La Jolla, CA) and dissolved in its vehicle solution (phosphate buffered saline). Y-27632 (1 mM) or vehicle solution was administered to the central cornea as a 3 μl drop by pipetting in a masked manner. Evaluation of IOP-lowering effect was performed by measuring the IOP with the tonometer at 1 hour after drug instillation.

Statistical Analysis of IOPs

Data are reported as means ± S.D. Two-tailed Student's t-test was used to compare between two groups of results. Differences between any two groups were regarded as significant when $P<0.01$(**) or $P<0.05$ (*).

Disease Associated Genome-Wide Analysis

One hundred clinically-diagnosed cases (male 46; female 54) with primary open-angle glaucoma over 30 years of age (mean age, 71.60 years; SD, 9.33 years) and non-glaucoma age-matched controls (mean age, 66.71 years; SD, 12.00 years) in a Japanese population were examined for this study. Informed consent was obtained from all participants, and the procedures used conformed to the tenets of the Declaration of Helsinki. Genomic DNAs were isolated from the peripheral blood of the POAG cases and age-matched controls for genotyping analysis. Genotyping was performed using the Affymetrix GeneChip Human Mapping 500 K Array Set (Affymetrix Services Laboratory, California). We omitted the SNP data under an 85% call rate, under 0.001 Hardy-Weinberg equilibrium (HWE), and under 5% minor allele frequency. Data analysis was performed using the LaboServer System (World Fusion, Tokyo Japan). An allelic frequency χ^2 test and genotypic frequency χ^2 test were calculated, respectively with respect to risk allele. The Odds ratio was calculated in three manners such as per allele odds ratio, heterozygote odds ratio, and homozygote odds ratio. Relative risk was also calculated, the same as for the odds ratio. The most significant SNPs were chosen in this report to evaluate the association of *VAV2*, *VAV3*, and *VAV1* in the cases.

Supporting Information

Figure S1 The comparison of intraocular pressures in age matched wild-type inbred C57BL/6 mice, wild-type littermate controls, and Vav2 and Vav3 heterozygous mice (Vav2$^{+/-}$, and Vav3$^{+/-}$). Intraocular pressures (IOPs) were measured using the TonoLab rebound tonometer for rodents from 6-week to 12-week, as described in the Methods. The phenotype of littermate wild-type mice was identical to that of the "inbred" C57BL/6 strain. The phenotype of Vav2 and Vav3 heterozygous mice were similar to that of wild-type. n = 20.
Found at: doi:10.1371/journal.pone.0009050.s001 (0.45 MB TIF)

Figure S2 The correlation between elevated IOP and angle changes in Vav2/Vav3-deficient mice. The IOP was measured in 7-week-old Vav2/Vav3-deficient (Vav2$^{-/-}$Vav3$^{-/-}$) mice (n = 20), followed by examination of the angle status by histology. While Vav2$^{-/-}$Vav3$^{-/-}$ mice with elevated IOP displayed histological evidence of angle closure, mice without elevated IOP showed either normal open angles or evidence of angle changes, angle closure or peripheral anterior synechiae. The mean and standard deviation of IOP in wild-type mice at 7-week-old (n = 18) were 13.7±3.12 mmHg, respectively. The 95th percentile of those

IOPs using a normal curve was 18.8 mmHg. IOP over 18.8 mmHg was regarded here as elevated IOP.
Found at: doi:10.1371/journal.pone.0009050.s002 (0.57 MB TIF)

Figure S3 Anti-myocilin staining of trabecular meshwork in Vav2/Vav3-deficient mice. Immunohistochemical staining of trabecular meshwork with anti-myocilin antibody in representative iridocorneal angle sections of age-matched wild-type and Vav2/Vav3-deficient ($Vav2^{-/-}Vav3^{-/-}$) 7-week-old mice with normal IOP, with either evidence of angle closure, or normal open angles similar to wild type mice. Myocilin (green-labeled), which is strongly expressed in TM cells, was regarded as a marker for TM cells. In $Vav2^{-/-}Vav3^{-/-}$ mice with angle closure, myocilin was not detected in the iridocorneal angle (indicated by arrows). Conversely, it was detected in sections from mice with normal open angles, similar to those in wild type mice. Blue fluorescence is DAPI counter staining. Scale bars, 20 um.
Found at: doi:10.1371/journal.pone.0009050.s003 (2.19 MB TIF)

Figure S4 Effects of ocular hypotensives in Vav2/Vav3-deficient mice. A. Ocular hypotensives used for human glaucoma, latanoprost, a prostaglandin analogue was tested in 7-week-old Vav2/Vav3-deficient ($Vav2^{-/-}Vav3^{-/-}$) mice with elevated IOP (n = 20). The IOP was measured 3 hours before and after topical application of 3 μl of 0.01% latanoprost in a masked manner. Vehicle was used as a control. Latanoprost lowered the IOP significantly in $Vav2^{-/-}Vav3^{-/-}$ mice (26.3±5.0 mmHg versus 15.8±5.1 mmHg; n = 20), while the IOP was not altered by the vehicle alone. The latanoprost-induced reduction of IOP in $Vav2^{-/-}Vav3^{-/-}$mice was statistically significant (**P<0.01, n = 20). The data shown are representative of three independent experiments performed. Error bars represent S.D. **P<0.01 versus vehicle-treated $Vav2^{-/-}Vav3^{-/-}$ mice. B. Using three different drugs for lowering IOP, we compared the effects by percentages of elevated IOP reduction. These data are representative from three independent experiments, respectively (n = 20). Error bars represent S.D. **P<0.01 versus vehicle-treated $Vav2^{-/-}Vav3^{-/-}$ mice. C. Rho-associated protein kinase Inhibitor, Y-27632 was tested for lowering IOP on $Vav2^{-/-}Vav3^{-/-}$ mice (n = 20). Y27632 administration has no effect against $Vav2^{-/-}Vav3^{-/-}$ mice (before, 19.69±4.98 mmHg; after, 18.83±5.60 mmHg; n = 20), while Y-27632 lowered the IOP significantly in age-matched wild-type mice (13.58±2.27 mmHg versus 12.31±1.94 mmHg; n = 20. p<0.05) and the IOP was not altered by the vehicle solution (13.25±1.71 mmHg versus 13.18±3.17 mmHg; n = 20). These data are representative from four independent experiments, respectively. Error bars represent S.D. *P<0.05 versus vehicle-treated WT mice.
Found at: doi:10.1371/journal.pone.0009050.s004 (0.41 MB TIF)

Figure S5 Sense probe staining for in situ hybridization experiments in ocular tissues. In situ hybridization with Vav2 and Vav3 sense probes were carried out as negative controls for the experiments. C57BL/6 mouse ocular tissue sections including the iridocorneal angle, sclera and cornea were used. With sense probes, there was no detectable signal around mouse iridocorneal angle tissues. TM; trabecular meshwork. Scl; sclera.
Found at: doi:10.1371/journal.pone.0009050.s005 (4.14 MB TIF)

Acknowledgments

The authors thank Professor Duco Hamasaki (Bascom Palmer Eye Institute, University of Miami School of Medicine, Florida) and Morton Smith, M.D. (Washington University Department of Ophthalmology & Visual Sciences) for helpful suggestions and discussion; and Mr. Tsutomu Osanai and Ms. Takae Oyama for technical help.

Author Contributions

Conceived and designed the experiments: KF TI KI. Performed the experiments: KF TI MA HK MF QC. Analyzed the data: KF TI KI MA MF MW EMB WAS. Contributed reagents/materials/analysis tools: KF TI KI MW WAS. Wrote the paper: KF KI EMB WAS.

References

1. Kass MA, Heuer DK, Higginbotham EJ, Johnson CA, Keltner JL, et al. (2002) The ocular hypertension treatment study: a randomized trial determines that topical ocular hypotensive medication delays or prevents the onset of primary open-angle glaucoma. Arch Ophthalmol 120: 701–713.
2. AGIS investigators (2002) The advanced glaucoma intervention study (AGIS): 7. The relationship between control of intraocular pressure and visual field deterioration. Am J Ophthalmol 130: 429–440.
3. Gabelt BT, Kaufman PL (2005) Changes in aqueous humor dynamics with age and glaucoma. Prog Retin Eye Res 24: 612–637.
4. Tan JC, Peters DM, Kaufman PL (2006) Recent developments in understanding the pathophysiology of elevated intraocular pressure. Curr Opin Ophthalmol 17: 168–174.
5. Bustelo XR (2001) Vav protein, adaptors and cell signaling. Oncogene 20: 6372–6381.
6. Schmidt A, Hall A (2002) Guanine nucleotide exchange factors for Rho GTPases: turning on the switch. Genes Dev 16: 1587–1609.
7. Turner M, Billadeau DD (2002) VAV proteins as signal integrators for multi-subunit immune-recognition receptors. Nat Rev Immunol 2: 476–486.
8. Swat W, Fujikawa K (2005) The Vav family: at the crossroads of signaling pathways. Immunol Res 32: 259–265.
9. Riteau B, Barber DF, Long EO (2003) Vav1 phosphorylation is induced byβ2 integrin engagement on natural killer cells upstream of actin cytoskeleton and lipid raft reorganization. J Exp Med 198: 469–474.
10. Gakidis MAM, Cullere X, Olson T, Wilsbacher JL, Zhang B, et al. (2004) Vav GEFs are required for β2 integrin-dependent functions of neutrophils. J Cell Biol 166: 273–282.
11. Holsinger LJ, Graef IA, Swat W, Chi T, Bautista DM, et al. (1998) Defects in actin-cap formation in Vav-deficient mice implicate an actin requirement for lymphocyte signal transduction. Curr Biol 8: 563–572.
12. Cella M, Fujikawa K, Tassi I, Kim S, Latinis K, et al. (2004) Differential requirements for Vav proteins in DAP10- and ITAM-mediated NK cell cytotoxicity. J Exp Med 200: 817–823.
13. Doody GM, Bell SE, Vigorito E, Clayton E, McAdam S, et al. (2001) Signal transduction through Vav-2 participates in humoral immune responses and B cell maturation. Nat Immunol 2: 542–547.
14. Faccio R, Teitelbaum SL, Fujikawa K, Chappel J, Zallone A, et al. (2005) Vav3 regulates osteoclast function and bone mass. Nat Med 11: 284–290.
15. Fujikawa K, Miletic AV, Alt FW, Faccio R, Brown T, et al. (2003) Vav1/2/3-null mice define an essential role for Vav family proteins in lymphocyte development and activation but a differential requirement in MAPK signaling in T and B cells. J Exp Med 198: 1595–1608.
16. Tybulewicz VLJ, Ardouin L, Prisco A, Reynolds LF (2003) Vav1: a key signal transducer downstream of the TCR. Immunol Rev 192: 42–52.
17. Karali A, Russell P, Stefani FH, Tamm ER (2000) Localization of myocilin/trabecular meshwork-inducible glucocorticoid response protein in the human eye. Invest Ophthalmol Vis Sci 41: 729–740.
18. Weinreb RN, Toris CB, Gabelt BT, Lindsey JD, Kaufman PL (2002) Effects of prostaglandins on the aqueous humor outflow pathways. Surv Ophthalmol 47 (suppl. 1): S53–S64.
19. Neufeld AH (1979) Experimental studies on the mechanism of action of timolol. Surv Ophthalmol 23: 363–370.
20. Pfeiffer N (1997) Dorzolamide: Development and clinical application of a topical carbonic anhydrase inhibitor. Surv Ophthalmol 42: 137–151.
21. Tanihara H, Inatani M, Honjo M, Tokushige H, Azuma J, et al. (2008) Intraocular pressure-lowering effects and safety of topical administration of a selective ROCK inhibitor, SNJ-1656, in healthy volunteers. Arch Ophthalmol 126: 309–315.
22. Rao PV, Peterson YK, Inoue T, Casey PJ (2008) Effects of pharmacologic inhibition of protein geranylgeranyltransferase type I on aqueous humor outflow through the trabecular meshwork. Invest Ophthalmol Vis Sci 49: 2464–2471.
23. Honjo M, Tanihara H, Inatani M, Kido N, Sawamura T, et al. (2001) Effects of Rho-associated protein kinase inhibitor, Y-27632, on intraocular pressure and outflow facility. Invest Ophthalmol Vis Sci 42: 137–144.
24. Pang IH, Clark AF (2007) Rodent models for glaucoma retinopathy and optic neuropathy. J Glaucoma 16: 483–505.
25. Aihara M, Lindsey JD, Weinreb RN (2003) Aqueous humor dynamics in mice. Invest Ophthalmol Vis Sci 44: 5168–5173.
26. Chang B, Smith RS, Hawes NL, Anderson MG, Zabaleta A, et al. (1999) Interacting loci cause severe iris atrophy and glaucoma in DBA/2J mice. Nat Genet 21: 405–409.

27. John SW, Smith RS, Savinova OV, Hawes NL, Chang B, et al. (1998) Essential iris atrophy, pigment dispersion, and glaucoma in DBA/2J mice. Invest Ophthalmol Vis Sci 39: 951–962.
28. Goldblum D, Kipfer-Kauer A, Sarra GM, Wolf S, Frueh BE (2007) Distribution of amyloid precursor protein and amyloid-beta immunoreactivity in DBA/2J glaucomatous mouse retinas. Invest Ophthalmol Vis Sci 48: 5085–5090.
29. Schlamp CL, Li Y, Dietz JA, Janssen KT, Nickells RW (2006) Progressive ganglion cells loss and optic nerve degeneration in DBA/2J mice is variable and asymmetric. BMC Neurosci 7: 66.
30. Anderson MG, Smith RS, Hawes NL, Zabaleta A, Chang B, et al. (2002) Mutations in genes encoding melanosomal proteins cuase pigmentary glaucoma in DBA/2J mice. Nat Genet 1: 81–85.
31. Nakano M, Ikeda Y, Taniguchi T, Yagi T, Fuwa M, et al. (2009) Three susceptible loci associated with primary open-angle glaucoma identified by genome-wide association study in a Japanese population. Proc Natl Acad Sci U S A 106(31): 12838–12842.
32. Tanito M, Minami M, Akahori M, Kaidzu S, Takai Y, et al. (2008) LOXL1 variants in elderly Japanese patients with exfoliation syndrome/glaucoma, primary open-angle glaucoma, normal tension glaucoma, and cataract. Mol Vis 14: 1898–1905.
33. Shibuya E, Meguro A, Ota M, Kashiwagi K, Mabuchi F, et al. (2008) Association of Toll-like receptor 4 gene polymorphisms with normal tension glaucoma. Invest Ophthalmol Vis Sci 49: 4453–4457.
34. Funayama T, Mashima Y, Ohtake Y, Ishikawa K, Fuse N, et al. (2006) SNPs and interaction analyses of noelin 2, myocilin, and optineurin genes in Japanese patients with open-angle glaucoma. Invest Ophthalmol Vis Sci 47: 5368–5375.
35. Inagaki Y, Mashima Y, Fuse N, Funayama T, Ohtake Y, et al. (2006) Polymorphism of b-adrenergic receptors and susceptibility to open-angle glaucoma. Mol Vis 12: 673–680.
36. Ishikawa K, Funayama T, Ohtake Y, Kimura I, Ideta H, et al. (2005) Association between glaucoma and gene polymorphism of endothelin type A receptor. Mol Vis 11: 431–437.
37. Jiao X, Yang Z, Yang X, Chen Y, Tong Z, et al. (2009) Common variants on chromosome 2 and risk of primary open-angle glaucoma in the Afro-Caribbean population of Barbados. Proc Natl Acad Sci U S A 106(40): 17105–17110.
38. Wolf C, Gramer E, Müller-Myhsok B, Pasutto F, Reinthal E, et al. (2009) Evaluation of nine candidate genes in patients with normal tension glaucoma: a case control study. BMC Med Genet 10: 91.
39. Narooie-Nejad M, Paylakhi SH, Shojaee S, Fazlali Z, Rezaei Kanavi M, et al. (2009) Loss of function mutations in the gene encoding latent transforming growth factor beta binding protein 2, LTBP2, cause primary congenital glaucoma. Hum Mol Genet 18(20): 3969–3977.
40. Sud A, Del Bono EA, Haines JL, Wiggs JL (2008) Fine mapping of the GLC1K juvenile primary open-angle glaucoma locus and exclusion of candidate genes. Mol Vis 4: 1319–1326.
41. Liu Y, Schmidt S, Qin X, Gibson J, Hutchins K, et al. (2008) Lack of association between LOXL1 variants and primary open-angle glaucoma in three different populations. Invest Ophthalmol Vis Sci 49(8): 3465–3468.
42. Thorleifsson G, Magnusson KP, Sulem P, Walters GB, Gudbjartsson DF, et al. (2007) Common sequence variants in the LOXL1 gene confer susceptibility to exfoliation glaucoma. Science 317(5843): 1397–1400.
43. Kumar A, Basavaraj MG, Gupta SK, Qamar I, Ali AM, et al. (2007) Role of CYP1B1, MYOC, OPTN, and OPTC genes in adult-onset primary open-angle glaucoma: predominance of CYP1B1 mutations in Indian patients. Mol Vis 13: 667–676.
44. Bill A, Svedberg B (1972) Scanning electron microscopic studies of the trabecular meshwork and the canal of Schlemm: an attempt to localize the main resistance to outflow of aqueous humor in man. Acta Ophthalmol 50: 295–320.
45. Wiedelholt M, Bielka S, Schweig F, Lütjen-Drecoll E, Lepple-Wienhues A (1995) Regulation of outflow rate and resistance in the perfused anterior segment of the bovine eye. Exp Eye Res 61: 223–234.
46. Filla MS, Woods A, Kaufman PL, Peters DM (2006) Beta1 and beta3 integrins cooperate to induce syndecan-4-containing cross-linked actin networks in human trabecular meshwork cells. Invest Ophthalmol Vis Sci 47(5): 1956–1967.
47. Peterson JA, Sheibani N, David G, Garcia-Pardo A, Peters DM (2005) Heparin II domain of fibronectin uses alpha4beta1 integrin to control focal adhesion and stress fiber formation, independent of syndecan-4. J Biol Chem 25 280(8): 6915–6922.
48. Diskin S, Cao Z, Leffler H, Panjwani N (2009) The role of integrin glycosylation in galectin-8-mediated trabecular meshwork cell adhesion and spreading. Glycobiology 19(1): 29–37.
49. Fukaya M, Hayashi Y, Watanabe M (2005) NR2 to NR3B subnit switchover of NMDA receptors in early postnatal motoneurons. Eur J Neurosci 21: 1432–1436.

OPEN ACCESS Freely available online

PLoS one

Modeling Retinal Degeneration Using Patient-Specific Induced Pluripotent Stem Cells

Zi-Bing Jin[1,2☯], Satoshi Okamoto[1☯], Fumitaka Osakada[3], Kohei Homma[1], Juthaporn Assawachananont[1], Yasuhiko Hirami[1], Takeshi Iwata[4], Masayo Takahashi[1,5*]

1 Laboratory for Retinal Regeneration, RIKEN Center for Developmental Biology, Kobe, Japan, **2** School of Optometry and Ophthalmology, Eye Hospital, Wenzhou Medical College, Wenzhou, China, **3** Systems Neurobiology Laboratory, The Salk Institute for Biological Studies, La Jolla, California, United States of America, **4** National Institute of Sensory Organs, National Hospital Organization Tokyo Medical Center, Tokyo, Japan, **5** Center for iPS Research and Application, Kyoto University, Kyoto, Japan

Abstract

Retinitis pigmentosa (RP) is the most common inherited human eye disease resulting in night blindness and visual defects. It is well known that the disease is caused by rod photoreceptor degeneration; however, it remains incurable, due to the unavailability of disease-specific human photoreceptor cells for use in mechanistic studies and drug screening. We obtained fibroblast cells from five RP patients with distinct mutations in the *RP1*, *RP9*, *PRPH2* or *RHO* gene, and generated patient-specific induced pluripotent stem (iPS) cells by ectopic expression of four key reprogramming factors. We differentiated the iPS cells into rod photoreceptor cells, which had been lost in the patients, and found that they exhibited suitable immunocytochemical features and electrophysiological properties. Interestingly, the number of the patient-derived rod cells with distinct mutations decreased *in vitro*; cells derived from patients with a specific mutation expressed markers for oxidation or endoplasmic reticulum stress, and exhibited different responses to vitamin E than had been observed in clinical trials. Overall, patient-derived rod cells recapitulated the disease phenotype and expressed markers of cellular stresses. Our results demonstrate that the use of patient-derived iPS cells will help to elucidate the pathogenic mechanisms caused by genetic mutations in RP.

Citation: Jin Z-B, Okamoto S, Osakada F, Homma K, Assawachananont J, et al. (2011) Modeling Retinal Degeneration Using Patient-Specific Induced Pluripotent Stem Cells. PLoS ONE 6(2): e17084. doi:10.1371/journal.pone.0017084

Editor: Mark Mattson, National Institute on Aging Intramural Research Program, United States of America

Received October 28, 2010; **Accepted** January 15, 2011; **Published** February 10, 2011

Funding: This study was supported by the grant from the Ministry of Health, Labour and Welfare, Japan (#H21-Nanchi-Ippan-216). The funders had no role in study design, data collection and analysis, decision to publish, or preparation of the manuscript.

Competing Interests: The authors have declared that no competing interests exist.

* E-mail: mretina@cdb.riken.jp

☯ These authors contributed equally to this work.

Introduction

Retinitis pigmentosa (RP) leads inevitably to visual impairment due to irreversible retinal degeneration, specifically of primary rod photoreceptors. The condition causes night blindness and visual field defects. The disease onset spans a wide range of ages, but RP most often occurs in late life. There is no treatment that allows patients to avoid deterioration of visual function. RP encompasses a number of genetic subtypes, with more than 45 causative genes and a large number of mutations identified thus far. The genetic heterogeneity of RP suggests a diversity of disease mechanisms, which remain largely unclear. Furthermore, for many of the RP subtypes, no appropriate animal models are available. Although large clinical trials have been conducted with α-tocopherol and β-carotene, these studies found no statistically significant change of visual function in RP patients [1,2]. The underlying mutations causing disease in the patients tested in the clinical trials were not revealed, and the variability of individual responses to these drugs is unknown. One of the reasons why these clinical trials failed to examine the effectiveness of drugs is that the effect of a drug may be different between patients with different underlying mutations.

Induced pluripotent stem (iPS) cells reprogrammed from somatic cells [3,4] have enabled us to easily generate patient-derived terminally differentiated cells *in vitro* [5–7]. We have successfully induced differentiation of photoreceptor cells from both human embryonic stem (ES) cells [8] and iPS cells [9,10]. Modeling pathogenesis and treatment *in vitro* using patient iPS cell-derived photoreceptors will elucidate disease mechanisms; circumvent problems related to differences among species that arise when using animal models; decrease patient risk; and reduce the cost of early-stage clinical trials. Here, we generated iPS cells from RP patients with different mutations and demonstrated the potential of patient-derived photoreceptors for disease modeling.

Materials and Methods

RP patients and genetic mutations

The protocol of this study adhered to the tenets of the Declaration of Helsinki. The study was approved by the ethical committees of the Institute of Biomedical Research and Innovation Hospital and the RIKEN Center for Developmental Biology, Japan. Written informed consent from all patients was obtained. We selected five RP patients from four families whose disease-causing mutations have been identified (**Fig. 1A–D and Fig. S1**). Of the five RP patients in this study, three late-onset patients carried the following mutations: 721Lfs722X in *RP1*, W316G in *PRPH2*, and G188R in *RHO*. Two relatively early-onset patients from the same family carried a H137L mutation in *RP9*, which we

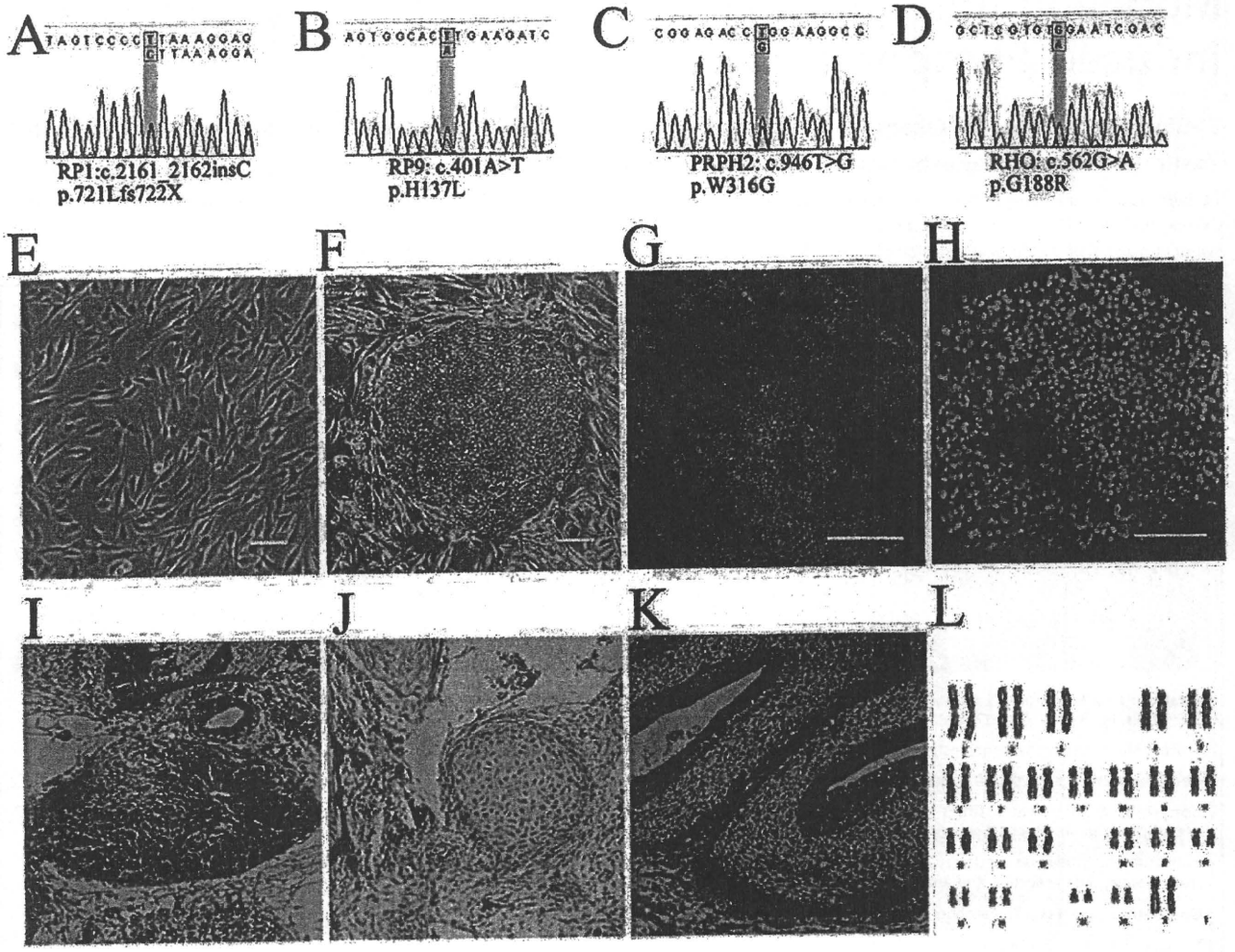

Figure 1. iPS cells derived from RP patients. Mutations identified in patients K21 (RP1) **(A)**, K11 and K10 (RP9) **(B)**, P101 (PRPH2) **(C)**, and P59 (RHO) **(D)**. Patient-derived fibroblast cells **(E)** were reprogrammed into iPS cells **(F)**. The iPS cells expressed SSEA-4 **(G)** and Nanog **(H)**. A teratoma formation test confirmed iPS cells' ability to generate all three germ layers: endoderm **(I)**, mesoderm **(J)** and ectoderm **(K)**. Karyotype analysis **(I)**. Scale bars, 50 μm.
doi:10.1371/journal.pone.0017084.g001

confirmed by both genomic and cDNA sequencing (**Fig. S2**). All patients showed typical manifestations of RP (**Tab. S1**). Peripheral blood obtained from patients was used for DNA isolation. A comprehensive screening of disease-causing genes was carried out as described previously [11]. For the RP9 mutation, total RNA was isolated from fresh blood samples and iPS cells, and synthesized cDNA was subjected to PCR and direct sequencing to confirm whether the mutation was located in the *RP9* gene or the pseudo-RP9 gene (paralogous variant). Both fibroblast and iPS cells were analyzed to re-confirm the identified mutation.

iPS cells generation

To generate iPS cells, retroviral transduction of Oct3/4, Sox2, Klf4, and c-Myc into patient-derived fibroblast cells was carried out as described previously [3]. Established iPS cell lines were maintained on a feeder layer of mitomycin C-treated SNL cells (a murine-derived fibroblast STO cell line expressing the neomycin-resistance gene cassette and LIF) in a humidified atmosphere of 5% CO_2 and 95% air at 37°C. Cells were maintained in DMEM-F12 supplemented with 0.1 mM non-essential amino acids, 0.1 mM 2-mercaptoethanol, 2 mM L-glutamine, 20% KnockOut Serum Replacement (KSR), and 4 ng/ml basic fibroblast growth factor (Upstate Biotechnology).

Transgene quantification

To examine the copy number of transgenes integrated into the host genome, DNA was isolated and quantitative detection of viral transgenes was performed using real-time PCR. The endogenous gene was used as a control. Before quantitative PCR, a standard curve for each primer and/or probe set was determined using a set of plasmid DNA dilutions. Taqman qPCR to detect integrated OCT3/4, KLF4, and MYC was performed using 20 μl reactions consisting of 10 μl TaqMan Master Mix with uracil N-glycosylase, 4.9 μM primers, 250 nM probe, and 1 μl of the DNA sample. Quantification of viral SOX2 was assayed using SYBR Green.

Teratoma formation

Animal protocols were approved by the RIKEN Center for Developmental Biology ethical committee (No. AH18-05). A total of 10^7 trypsinized iPS cells were injected subcapsularly into the testis of SCID mice (two mice per iPS cell line). Four weeks later, the testis was fixed and sectioned for H&E staining.

Immunocytochemistry

Cells were fixed with 4% paraformaldehyde for 15 min at 4°C and then permeabilized with 0.3% Triton X-100 for 45 min. After 1 h blocking with 5% goat serum, cells were incubated with primary antibodies overnight at 4°C and subsequently with secondary antibodies for 1 h at room temperature. The primary and second antibodies used are listed in **Tab. S2**.

Karyotype analysis

Karyotype analysis of the iPS cell chromosomes was carried out using a standard G-band technique (300–400 band level).

Photoreceptor differentiation and drug testing

In vitro differentiation of rod photoreceptor cells was performed as previously reported [8], but with a minor modification. To find a KSR optimal for retinal differentiation, lot testing was conducted before differentiation. iPS colonies were dissociated into clumps with 0.25% trypsin and 0.1 mg/ml collagenase IV in PBS containing 1 mM $CaCl_2$ and 20% KSR. Feeder cells were removed by incubation of the iPS cell suspension on a gelatin-coated dish for 1 h. iPS clumps were moved to a non-adhesive MPC-treated dish (NUNC) in maintenance medium for 3 days, in 20% KSR-containing differentiation medium (DMEM-12 supplemented with 0.1 mM non-essential amino acids, 0.1 mM 2-mercaptoethanol, 2 mM L-glutamine) for 3 days, then in 15% KSR-containing differentiation medium for 9 days, and finally in 10% KSR-containing medium for 6 days. Cells were treated with Lefty-A and Dkk-1 during floating culture. At day 21, the cells were plated en bloc on poly-D-lysine/laminin/fibronectin−coated 8-well culture slides (BD Biocoat) at a density of 15–20 aggregates/cm^2. The cells were cultured in 10% KSR-containing differentiation medium until day 60. Cells were further treated with 100 nM retinoic acid (Sigma) and 100 μM taurine (Sigma) in photoreceptor differentiation medium (GMEM, 5% KSR, 0.1 mM non-essential amino acids, 0.1 mM 2-mercaptoethanol, 1 mM pyruvate, N2 supplement, and 50 units/ml penicillin, 20 μg/ml streptomycin). Differentiated cells from both normal and patient iPS cells were treated with 100 μM α-tocopherol, 200 μM ascorbic acid and 1.6 μM β-carotene starting at differentiation day 120. One week later, cells were fixed for immunostaining.

Electrophysiological recording

Recombinant lentiviral vectors expressing GFP under the control of the Nrl or RHO promoters were generated in HEK293t cells (RIKEN Cell Bank), and differentiated cells were infected with virus on day 90. Cells expressing GFP were targeted for patch clamp recordings. Voltage-clamp recordings were performed with 12–15 MΩ glass electrodes. Signals were amplified using Multiclamp 700B amplifiers (Molecular Devices). The internal solution was 135 mM K-gluconate, 10 mM HEPES, 3 mM KCl, 0.2 mM EGTA, 2.5 mM $MgCl_2$, 5 mM adenosine 5′-triphosphate, 0.3 mM guanosine-5′-triphosphate, 0.06 mM Alexa Fluor 594 (Molecular probes), adjusted to pH 7.6 with KOH. The retinal cells were perfused with oxygen-bubbled external medium: 23 mM $NaHCO_3$, 0.5 mM KH_2PO_4, 120 mM NaCl, 3.1 mM KCl, 6 mM Glucose, 1 mM $MgSO_4$, 2 mM $CaCl_2$, and 0.004% Phenol red. The medium was heated to 37°C with a temperature controller (Warner Instruments).

Cell count and statistical analysis

Differentiated cells visualized with specific antibodies were counted blindly by an independent observer. Data are expressed as means ± s.e.m. The statistical significance of differences was determined by one-way ANOVA followed by Tukey's test or Dunnett's test, or by two-way ANOVA followed by Bonferroni test using the GraphPad Prizm software. Probability values less than 0.05 were considered significant.

Results

Generation of iPS cell lines from patients with RP

Mutations identified in the five patients were confirmed by bi-directional sequencing (**Fig. S1**). Through genotyping of four patients and two normal relatives in the RP9 family, we found the H137L mutation in the *RP9* gene co-segregated with the disease, strongly indicating that the mutation is indeed the genetic cause of the disease. We cultured fibroblasts from skin samples of these patients on gelatin-coated dishes (**Fig. 1E**) and infected them with retroviral vectors encoding *OCT3/4* (also known as *POU5F1*), *SOX2*, *KLF4*, and *c-MYC*, using a previously established method [3]. Each mutation was re-confirmed in both fibroblasts and iPS cells. Established iPS colonies showed human embryonic stem cell-like morphology (**Fig. 1F and Fig. S3A**) and expressed pluripotency markers (**Fig. 1C–D**). We selected iPS cell lines for each patient using multiple criteria. First, we excluded iPS cell lines in which spontaneous differentiation occurred repeatedly during maintenance (**Fig. S3B**). We chose iPS colonies that maintained morphologies similar to those of human ES cells through more than 10 passages. Second, we quantified the transgene copy number and selected iPS cell lines with the fewest integrations, as the risk of gene disruption through random insertion increases with the number of transgenes (**Fig. S4A–E**). Third, in order to select iPS cell lines with full pluripotency, we verified the ability to form teratomas. Teratomas formed by injecting iPS colonies into the testis *in vivo* showed contributions to all three embryonic germ layers: ectoderm, mesoderm, and endoderm (**Fig. 1E–G**). Finally, karyotype analysis was carried out to examine the chromosome integrity. The patient-iPS cells showed normal karyotypes after extended passage, indicating chromosomal stability (**Fig. 1H**). These results provide *in vitro* and *in vivo* functional proof of pluripotency for RP patient-derived iPS cells.

Generation of patient-specific retinal photoreceptor

We previously demonstrated *in vitro* differentiation of retinal photoreceptor cells from wild-type human ES [8] and iPS cells [9,10] using a stepwise differentiation method known as serum-free culture of embryoid body-like aggregates [12]. We first evaluated the differentiation efficiency of three selected iPS cell lines of the five patients (**Fig. 2A**). Retinal progenitor, photoreceptor precursor, retinal pigment epithelium (RPE) and rod photoreceptor cells were sequentially induced (**Fig. 2B–K**), consistent with our previous studies [8–10,12]. All patient-derived iPS cell lines differentiated into RPE cells that form ZO-1+ tight junctions on differentiation day 60, with timing, morphology, and efficiency similar to that of wild-type iPS cells (**Fig. 2D–E; Fig. S5**). Immature photoreceptors expressing Crx and Recoverin (day ~60) were observed as clusters in the colonies (**Fig. S6A–B**). The patient-iPS cells also differentiated into blue Opsin+ or red/green Opsin+ cone photoreceptor cells (**Fig. 2H** and data not shown). Immunostaining of Rhodopsin (a marker of mature rod photoreceptors) revealed no Rhodopsin+ cells at differentiation day 100 (data not shown). Rhodopsin+ cells appeared at differentiation day 120 with a stable efficiency of the three independent iPS cell lines from each patient (**Fig. 2K,N and Fig. S6C**). Additionally, 15.1±0.60% and 13.3±1.65% cells were positive for Recoverin (a conventional marker for both rod, cone photoreceptors and cone bipolar cells) in K21- and K11-iPS cells, respectively

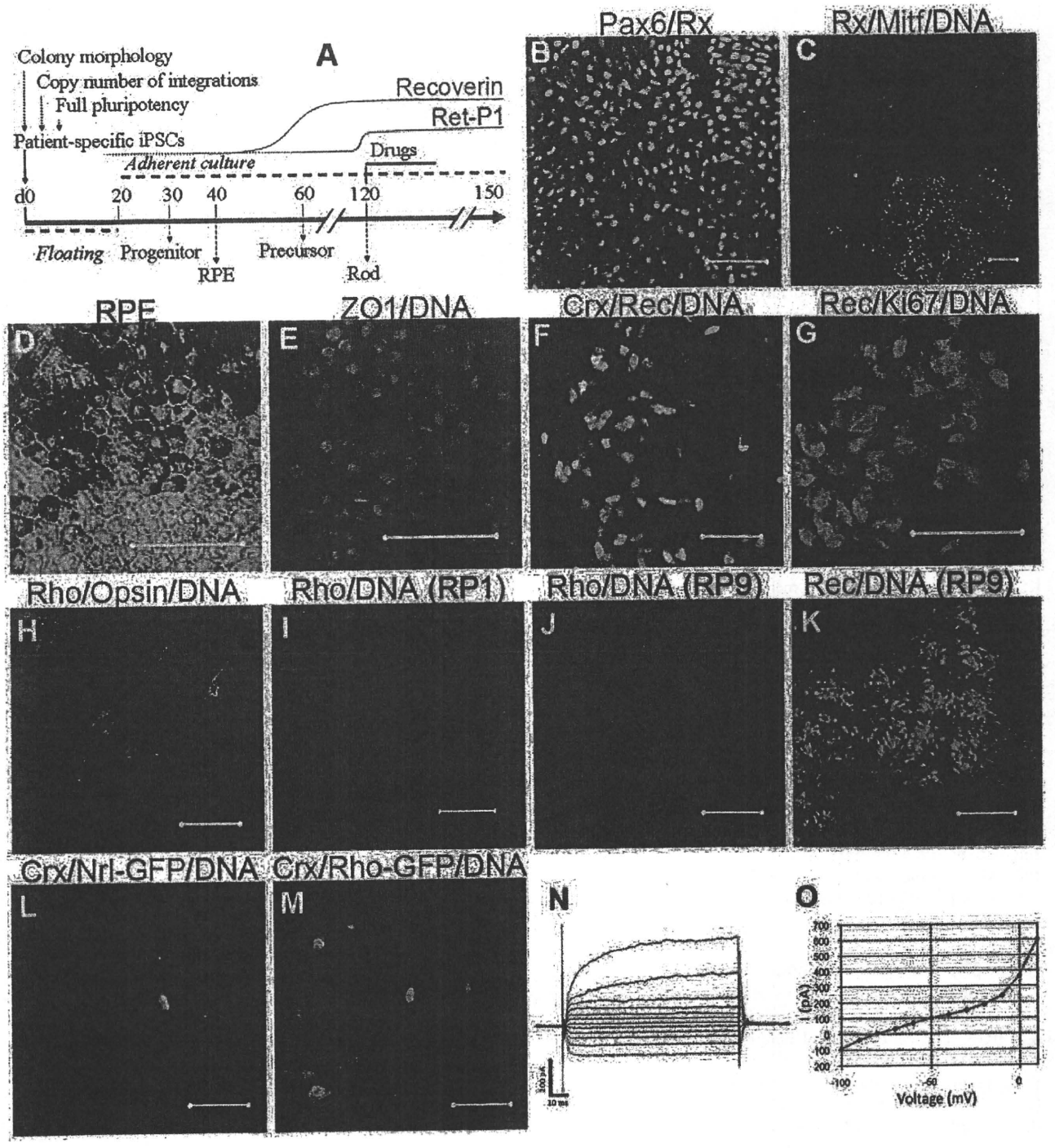

Figure 2. Induction of patient-specific retinal photoreceptor cells. Retinal cells were induced sequentially by *in vitro* differentiation. **(A)** Experimental schema. **(B)** Neural retina progenitor cells (Pax6+Rx+) and RPE progenitor cells (Mitf+) were separated in the culture dish **(C)**. Patient-specific RPE cells exhibited hexagonal morphology and pigmentation **(D)** and expressed the tight junction marker ZO-1 **(E)**. Photoreceptor cells were positive for immature photoreceptor markers Crx and Recoverin on day 60 **(F)**. Recoverin+ cells did not co-express Ki67, a proliferating cell marker **(G)**. Differentiation of rod photoreceptors (Rhodopsin+) and cone photoreceptors (Opsin+) from patient iPS cells **(H)**. Rhodopsin + rod photoreceptors induced from K21-iPS at day 120 **(I)**. K11-derived rod photoreceptors were observed at day 120 **(J)**. No Rhodopsin+ cells were detected, but Recoverin+ cells were present at day 150**(K)**. Induced rod photoreceptor cells (Crx+) labeled with lentiviral vectors encoding GFP driven by a rod photoreceptor-specific promoter Nrl **(L**: Nrl-GFP) or Rhodopsin **(M**: Rho-GFP). Arrows indicate cells co-expressing Crx and GFP. **(N)** Whole-cell recording of rod photoreceptor cell differentiated human iPS cells. Recorded cells expressed GFP under the control of the Rhodopsin promoter. **(O)** Relationship between voltage and membrane current (i) produced a non-linear curve, suggesting that voltage-dependent channels exist in iPS cell-derived rod photoreceptors Rec, Recoverin; Rho, Rhodopsin. Scale bars, 50 μm.
doi:10.1371/journal.pone.0017084.g002